Spectral Analysis of Heart Rate Variability in Time-Varying Conditions and in the Presence of Confounding Factors

Leif Sörnmo, *Fellow, IEEE*, Raquel Bailón, and Pablo Laguna, *Fellow, IEEE*

(Methodological Review)

***Abstract*—The tools for spectrally analyzing heart rate variability (HRV) has in recent years grown considerably, with emphasis on the handling of time-varying conditions and confounding factors. Time–frequency analysis holds since long an important position in HRV analysis, however, this technique cannot alone handle a mean heart rate or a respiratory frequency which vary over time. Overlapping frequency bands represents another critical condition which needs to be dealt with to produce accurate spectral measurements. The present survey offers a comprehensive account of techniques designed to handle such conditions and factors by providing a brief description of the main principles of the different methods. Several methods derive from a mathematical/statistical model, suggesting that the model can be used to simulate data used for performance evaluation. The inclusion of a respiratory signal, whether measured or derived, is another feature of many recent methods, e.g., used to guide the decomposition of the HRV signal so that signals related as well as unrelated to respiration can be analyzed. It is concluded that the development of new approaches to handling time-varying scenarios are warranted, as is benchmarking of performance evaluated in technical as well as in physiological/clinical terms.**

***Index Terms*—Heart rate variability, time-varying analysis, confounding factors, spectral analysis, redefinition of frequency bands, respiration-guided decomposition.**

I. Introduction

RESEARCH on heart rate variability (HRV) has over the years expanded to become a genuinely multidisciplinary area which today includes a wide range of engineering aspects as well as innumerable physiological and clinical applications. In spite of the expansion, the basis of HRV analysis remains as modest as it was in the very first studies published some 50 years ago, namely an RR interval series obtained from the single-lead ECG. The simple, noninvasive recording procedure is likely one of several reasons why HRV analysis has gained such widespread popularity.

By analyzing the ever-present beat-to-beat changes in heart rate, the complex interaction between the parasympathetic and sympathetic branches of the autonomic nervous system (ANS) on the sinoatrial node can be assessed indirectly. In healthy subjects, the instantaneous heart rate represents the net effect of the neural output of the two branches, causing the heart rate to adjust itself to the subject's current situation; heart rate is decreased by parasympathetic stimulation and increased by sympathetic stimulation. Impaired interaction between the two branches is often reflected by a reduced HRV associated with cardiovascular risk factors and disease states, including hypertension, heart failure, diabetes, and obesity [1]. However, the relevance of HRV analysis goes far beyond the understanding of somatic conditions as its popularity in social, psychological, and behavioral research has grown considerably in recent years for the purpose of assessing, e.g., mental stress, cognitive performance, fitness and sports performance [2], [3].

The information carried by the RR interval series need to be translated to a set of indices reflecting, among other physiological mechanisms, the interaction between the parasympathetic and sympathetic branches—a translation problem which has received much attention in the realm of engineering. The simplest approach to HRV analysis is to compute univariate statistical dispersion measures of the RR interval series. Since such measures are blind to the rhythmical variation in heart rate, power spectral analysis was introduced at an early stage of the history of HRV analysis [4], [5], [6], [7], later to become the preferred approach in clinical studies. Since the RR interval series is sampled at irregular time instants, equidistant resampling has to be performed to allow proper interpretation of the power spectrum, unless the spectral method is designed to handle irregularity [8]. By computing the power of different frequency bands (very low frequency, VLF, 0.0033–0.04 Hz; low frequency, LF, 0.04–0.15 Hz; high frequency, HF, 0.15–0.40 Hz), information on the ANS can be inferred. For example, it has been shown

Manuscript received 19 April 2022; revised 17 October 2022; accepted 30 October 2022. Date of publication 8 November 2022; date of current version 15 January 2024. This work was supported by the Royal Physiographic Society, Lund, Sweden, and CIBER in Bioengineering, Biomaterials & Nanomedicne (CIBERBBN) through Instituto de Salud Carlos III and FEDER (Spain), funded by MICINN and FEDER, Gobierno de Aragón (Reference Group BSICoS T39-17R) co-funded by FEDER 2014-2020 "Building Europe from Aragón" under Projects PID2019-104881RB-I00 and PID2019105674RB-I00. *(Corresponding author: Leif Sörnmo.)*

Leif Sörnmo is with the Department of Biomedical Engineering, Lund University, 22100 Lund, Sweden (e-mail: leif.sornmo@bme.lth.se).

Raquel Bailón and Pablo Laguna are with the BSICoS Group, Aragón Institute of Engineering Research, University of Zaragoza, and Centro de Investigación Biomédica en Red en Bioingeniería Biomateriales y Nanomedicina (CIBER-BBN), 50015 Zaragoza, Spain (e-mail: rbailon@unizar.es; laguna@unizar.es).

Digital Object Identifier 10.1109/RBME.2022.3220636

that the HF band mainly reflects efferent vagal activity due to respiratory activity since total vagal blockade essentially cancels the power of this band [6], [7], [9]. On the other hand, the LF band is influenced by both parasympathetic and sympathetic activity, making its interpretation more complicated. The interpretation of the VLF band involves additional mechanisms related to long-term regulation, e.g., thermoregulation. However, correct interpretation of the VLF band calls for stationary, long-term recordings, which are very difficult to obtain.

The relevance of spectral analysis is not only related to whether a frequency band reflects a certain dynamic of the ANS, but also whether the RR interval series can be treated as a stationary process—an assumption implicit to power spectral analysis. In practice, this assumption rarely holds, and less so as the ECG recording becomes increasingly longer [10]. Rather than employing a statistical test on stationarity [11], [12], the relevance of spectral analysis is often, though not always, judged from the context in which the ECG is recorded. Time–frequency analysis is the preferred approach when recordings made under nonstationary conditions are to be analyzed, e.g., physical activity and autonomic response to provocation including deep breathing, exercise stress testing, ambulatory monitoring, Valsalva maneuver, and head-up tilt [13], [14], [15].

An entire ecosystem of indices has grown up aiming to provide information on the nonlinear dynamics of RR intervals, which makes it possible to capture information of physiological and diagnostic significance. Long-range correlation and fractal analysis, short-term complexity, entropy and regularity, nonlinear dynamical systems and chaotic behavior, as well as many other aspects have been explored [16], [17], [18].

A number of confounding factors of electrophysiological and mechanical origin influencing the RR interval series render the assessment of HRV complicated, irrespective of whether linear or nonlinear techniques are used. The following factors have been treated to various extents in the literature:

- presence of occasional ectopic beats,
- influence of a time-varying mean heart rate,
- aliasing at low mean heart rates,
- respiration and frequency band definitions,
- overlapping frequency bands, and
- non-neural and mechanical mechanisms, including atrial stretching due to respiration and cardiolocomotor coupling.

Of these factors, handling of occasional ectopic beats has received by far the most attention, whereas handling of the other factors have been addressed in few studies and then usually in combination with time–frequency analysis.

Numerous technical reviews and surveys have been published covering aspects of HRV analysis with different emphasis: historical perspective [19], [20], mainstream analysis [21], [22], [23], [24], [25], [26], [27], [28], [29], [30], spectral and time–frequency analysis [1], [14], [15], and nonlinear dynamics analysis [16], [17]. The main motivation behind the present survey is to provide an account of methods developed for spectral HRV analysis in time-varying conditions, often characterized as nonstationary, and how the above-mentioned confounding factors are handled largely by model-based approaches—a survey which so far is missing. To substantiate the presentation, the main principles of the different models and methods particularly developed for HRV analysis are briefly described. Significant inspiration is drawn from the block diagram in Fig. 1 consisting of two main blocks: a simple, conceptual model for RR interval generation and the main signal processing methods which together form HRV analysis. The sinoatrial node model is assumed to have a mathematical structure well suited to propel the design of signal processing methods. The other blocks of the conceptual model are treated as black boxes whose output are to be inferred from the RR intervals. Respiratory information is either measured by a dedicated sensor or derived from the ECG, e.g., [31], [32], [33], [34], [35], [36], [37], [38]. This type of modeling has helped provide significant knowledge on the nature of HRV, conveyed by a variety of indices characterizing ANS activity. However, as knowledge on the interaction between the ANS and the cardiovascular system becomes more advanced, the modeling may turn out too simplistic, calling for further development to agree with the well-known aphorism that "models should be made as simple as possible, but not simpler".

Mathematical modeling of the sinoatrial node can take place at the cellular level, then accounting for ionic propagation mechanisms in cardiac tissue [39], [40]; however, such low-level modeling is ill-suited as a springboard for developing signal processing methods and therefore not considered here. Neither are the many techniques for time–frequency analysis considered here, the interested reader is referred to, e.g., [14], [15], [41], for further information.

The survey is organized as follows. Section II describes sinoatrial node models suitable for simulation as well as for developing heart rhythm representations (Section III) and methods for correction of occasional ectopic beats (Section IV). Section V deals with spectral analysis in time-varying conditions, notably redefinition of the HF band using respiratory information and handling of spurious spectral components observed during exercise stress testing. Sections VI and VII deal with time–frequency based parameter estimation and signal decomposition, respectively, where both techniques are guided by respiration. Finally, Section VIII discusses different approaches to improving HRV spectral analysis.

II. Modeling of the Sinoatrial Node

Different models have been proposed for generating variability in heart rate, either by accounting for certain characteristics of physiological relevance or using a statistical law whose relevance is assessed by how well the model output fits real data. Depending on model flexibility, various time-varying conditions can be handled, including changes in mean heart rate, HRV spectrum, and short- and long-term behavior. The output of a sinoatrial node model is a series of event times at which the node fires off an electrical impulse,

$$t_0, t_1, \ldots, t_M,$$

or, alternatively, a series of interevent intervals, i.e., a series of modeled RR intervals,

$$r_k = t_k - t_{k-1}, \qquad k = 1, 2, \ldots, M. \tag{1}$$

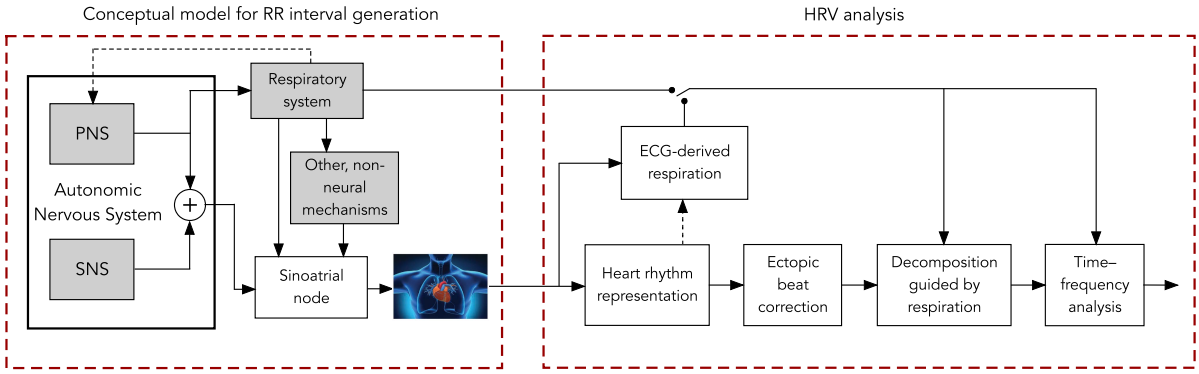

Fig. 1. A simple, conceptual model for RR interval generation and the main signal processing blocks of HRV analysis. RR interval generation is here synonymous to a mathematical model of the sinoatrial node which outputs a series of the event times. The activities of the shaded blocks play an important role in HRV analysis and interpretation, though they are not subject to mathematical modeling. QRS detection and beat classification are here considered part of heart rhythm representation, information which is used for ECG-derived respiration (dashed arrow); their description is beyond the scope of the present survey.

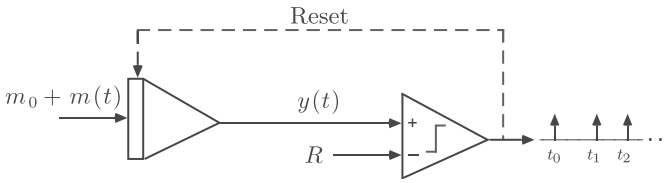

Fig. 2. The integral pulse frequency modulation (IPFM) model, with the input function $m_0 + m(t)$ that modulates the variability of interevent intervals, resulting in the event series $t_0, t_1, \ldots$.

The first event is assumed to occur at time $t_0 = 0$, which also defines the onset of the observation interval.

In this section, three models are described with a counterpart in signal processing in the sense that the parameters can be estimated using either statistical or deterministic inference. Clearly, the models can be used for simulating RR interval series, of particular value when testing and evaluating performance. In such cases, the model parameters are either chosen based on a priori information or inferred from real data.

A. IPFM Modeling

The time-invariant integral pulse frequency modulation (IPFM) model is by far the most popular model for generating an event series, probably explained by its simplicity and yet physiological relevance, see, e.g., [42], [43], [44], [45], [46], [47], [48], [49], [50], [51], [52], [53], [54], [55], [56], [57], [58], [59], [60], [61], [62], [63], [64]. The model input is composed of a DC level m_0, defining the repetition rate of events, and a modulating, zero-centered signal $m(t)$, defining the variability of interevent intervals. An event is generated at t_k when the integral of the input reaches the threshold R,

$$\int_{t_{k-1}}^{t_k} (m_0 + m(\tau))d\tau = R, \quad k = 1, \ldots, M. \tag{2}$$

The integrator is then reset to zero, the integration is repeated, a new event is generated, and so on, see Fig. 2.

In physiological terms, $m(t)$ determines the variability in heart rate as modulated by autonomic activity on the sinoatrial node, the integrator output $y(t)$ corresponds to charging of the membrane potential of a sinoatrial pacemaker cell. By setting $m_0 = 1$, the expression in (2) becomes

$$\int_{t_0=0}^{t_k} \frac{1 + m(\tau)}{T} d\tau = k, \quad k = 1, \ldots, M, \tag{3}$$

where R has been renamed to T as it now represents the mean interevent interval. Since the variability is much smaller relative to the mean heart rate, $m(t)$ is assumed to satisfy $|m(t)| \ll 1$.

The modulating signal $m(t)$ has been defined as a weighted sum of two sinusoids, representing the sympathetic and parasympathetic respiratory oscillators. The two weights are either set to fixed values [50], [55], or given a time-varying structure [63]. The sinusoidal definition of $m(t)$ has been employed for testing different rhythm representations and spectral analysis techniques [44], [45], [50], [52], [55], [59]. A more realistic approach is to estimate $m(t)$, e.g., using the heart timing representation of RR intervals described in Section III-A, accompanied by estimation of the parameters of a linear, stochastic model like the autoregressive (AR) model. By feeding the identified model with white, Gaussian noise, its output exhibits the same spectral characteristics as the estimate $\hat{m}(t)$ and therefore can serve as $m(t)$ [50], [61], [62].

When the input $1 + m(t)$ is defined by white, Gaussian noise, the IPFM model loses some of its physiological relevance. Nonetheless, this case deserves attention as it constitutes the basis of history-dependent point process modeling, see Section II-C. The integrator output is given by

$$y(t) = t + w(t), \tag{4}$$

where $w(t)$ is integrated white noise with variance σ_m^2. The output $y(t)$ is known as a Wiener process with positive drift. The time required for $y(t)$ to reach T for the first time is a random variable r described by the inverse Gaussian probability density

function (PDF) [65],

$$p(r;\mu,\lambda)=\sqrt{\frac{\lambda}{2\pi r^3}}\exp\left[-\frac{\lambda(r-\mu)^2}{2\mu^2 r}\right], \tag{5}$$

whose mean μ and shape $\lambda>0$ can be expressed in terms of the parameters defining $m(t)$ and T,

$$\mu=T,\quad \lambda=\frac{T^2}{\sigma_m^2}. \tag{6}$$

The resulting event series is a renewal process where the inter-event intervals are statistically independent and identically distributed. Such a process is history-independent and cannot account for the effect of sympathetic and parasympathetic input to the sinoatrial node which is known to last for several RR intervals.

A major limitation of the time-invariant IPFM model is that a fixed T implies a constant heart rate. Since this is unrealistic in HRV applications where the heart rate changes over time, e.g., during exercise stress testing, the time-varying IPFM model should be considered [66], [67], meaning that

$$T\rightarrow T(t).$$

B. Filtered-Noise Modeling

Another approach to modeling RR intervals is to filter white, Gaussian noise using a linear, time-invariant system, so that the spectral characteristics of the output series of interevent intervals resemble those of real data. Thus, in contrast to the IPFM model, this approach does not pretend to mimic sinoatrial node physiology. While the filtered-noise model has been much less considered for simulation purposes [68], even so, its relevance is demonstrated by the many studies in which this model represents the basis of HRV spectral analysis. The time-invariant AR model, introduced for HRV analysis in [69], is the most popular, defined by

$$r_k=-a_1r_{k-1}-\cdots-a_pr_{k-p}+v_k, \tag{7}$$

where v_k is white noise with variance σ_v^2. Since white noise by definition is zero-mean, the mean interevent interval T needs to be added to r_k to produce realistic data and become the interevent interval defined in (1). The variance σ_v^2 must be chosen such that the variance of r_k is much smaller than T. The coefficients $a_1,\ldots,a_p$, the model order p, and T is either predetermined or estimated from data.

A bimodal, Gaussian power spectrum has been proposed to model RR intervals, where one Gaussian accounts for respiratory sinus arrhythmia and another for baroreflex regulation [70]. This model may indeed be approximated by (7) since the two Gaussians can largely be modeled by a fourth-order AR model, where the proximity of the poles to the unit circle determines the width of the Gaussian-like bells.

In the time-varying version of the AR model, $a_1,\ldots,a_p$, and T are replaced by their time-varying counterparts $a_{1,k},\ldots,a_{p,k}$, and T_k. By analogy with the time-invariant AR model, the time-varying model has mainly served as the basis for time–frequency analysis [13], [14], [71], [72], [73], [74], [75]. An exception is the time-varying autoregressive, moving average (ARMA) model proposed for simulation [76]: the dominant frequencies and the powers defining the LF and HF components are controlled by varying the locations of the poles and the zeros according to some predefined pattern. For example, piecewise linear functions were used to model changes observed during exercise stress testing and music-induced emotions. It should be noted that filtered-noise modeling can be used to simulate RR intervals as well as heart rate.

C. History-Dependent Point Process Modeling

A point process is a stochastic model of the next event time t_{k+1} given that the history, i.e., the previous event times $t_0,\ldots,t_k$, is known. This process can be defined in several ways of which one straightforward is to specify the PDF of the next interevent interval. In the pioneering study [77], a point process model was proposed for HRV analysis, where the choice of PDF was inspired by the IPFM model and the associated inverse Gaussian PDF. History-dependence is introduced by modeling the mean as an autoregression of the p previous interevent intervals, cf. (7),

$$\mu_{\mathrm{RR}}=\mu(\mathcal{H}_k,\mathbf{a})=a_0+\sum_{i=1}^{p}a_ir_{k-i+1}, \tag{8}$$

where $\mathcal{H}_k=(r_{k-p+1},\ldots,r_k)$ is the event history and the vector $\mathbf{a}$ contains the $p+1$ regression parameters. Thus, the PDF of the next interevent interval $t-t_k$ is given by

$$p(t-t_k;\mu(\mathcal{H}_k,\mathbf{a}),\lambda)=\sqrt{\frac{\lambda}{2\pi(t-t_k)^3}}\exp\left[-\frac{\lambda(t-t_k-\mu(\mathcal{H}_k,\mathbf{a}))^2}{2\mu^2(\mathcal{H}_k,\mathbf{a})(t-t_k)}\right], \tag{9}$$

where $t>t_k$. The related standard deviation is given by

$$\sigma_{\mathrm{RR}}=\sqrt{\frac{\mu^3(\mathcal{H}_k,\mathbf{a})}{\lambda}}. \tag{10}$$

Note that the scalar p denotes model order whereas the function $p(\cdot)$ denotes a PDF.

Although the model parameters $(\mathbf{a},\lambda)$ do not depend explicitly on time, suggesting that the interevent intervals represent a stationary process, parameter estimation can be performed locally to produce time-varying estimates which account for nonstationarity [77]. Consequently, when simulating RR intervals using (8) and (9), $(\mathbf{a},\lambda)$ can be held fixed or made to vary over time according to some predefined pattern. The model order p has been treated as fixed over time, determined from real data using the Akaike information criterion in combination with a statistical goodness-of-fit test.

In contrast to the IPFM and filtered-noise models, the PDF in (9), modeling RR intervals, is easily modified to model heart rate using the random variable s and the following transformation of t [77],

$$s=\frac{c}{t-t_k}, \tag{11}$$

where $c = 60$ s/min converts interval to rate, expressed in events per minute. The resulting PDF is given by

$$p(s;\mu(\mathcal{H}_k,\mathbf{a}),\lambda) = \sqrt{\frac{c^{-1}\lambda}{2\pi s}}\exp\left[-\frac{\lambda(1-c^{-1}\mu(\mathcal{H}_k,\mathbf{a})s)^2}{2c^{-1}\mu^2(\mathcal{H}_k,\mathbf{a})s}\right] \tag{12}$$

and the related mean and standard deviation by

$$\mu_{\text{HR}} = c\left(\frac{1}{\mu(\mathcal{H}_k,\mathbf{a})}+\frac{1}{\lambda}\right), \tag{13}$$

$$\sigma_{\text{HR}} = \sqrt{\frac{2\mu(\mathcal{H}_k,\mathbf{a})+\lambda}{\mu(\mathcal{H}_k,\mathbf{a})c^{-2}\lambda^2}}, \tag{14}$$

respectively.

Just because the inverse Gaussian model originates from the IPFM model (when fed with white, Gaussian noise) does not necessarily make it physiologically relevant for simulation of RR intervals and heart rate. To shed light on its relevance, the inverse Gaussian model was therefore compared to the Gaussian, lognormal, and gamma models, all four models defined by time-varying parameters [78]. Using the Kolmogorov–Smirnov test, the inverse Gaussian model was found to provide the overall best goodness-of-fit to data recorded during a pharmacological autonomic blockade protocol.

III. Model-Based Heart Rhythm Representations

The interval tachogram $d_{\text{IT}}(k)$, i.e., r_k, and the inverse interval tachogram $d_{\text{IIT}}(k)$, i.e., the instantaneous heart rate, are classical representations of heart rhythm. While these HRV signals have been used extensively in time domain analysis of HRV, they suffer from the disadvantage of being functions of k, not of t, and therefore ill-suited for spectral analysis. To allow the results to be expressed in hertz, as well as to facilitate joint analysis of heart rate and other physiological signals, $d_{\text{IT}}(k)$ and $d_{\text{IIT}}(k)$ are transformed into their continuous-time counterparts known as the interval function $d_{\text{IF}}(t)$ and the inverse interval function $d_{\text{IIF}}(t)$, respectively. Using interpolation between the samples positioned at the event times t_k, an evenly sampled signal is obtained at the desired rate [24]. Other useful representations include the event series $d_{\text{E}}(t)$, defined as a sum of delta functions positioned at the event times, and its lowpass filtered version $d_{\text{LE}}(t)$.

While these six heart rhythm representations are intuitive, none is derived from a sinoatrial node model. In this section, two time-varying representations are described, both based on the IPFM model, namely the heart timing signal and a set of signals derived from the history-dependent point process model. The former signal is derived by deterministic reasoning, whereas the latter set of signals by statistical inference.

A. The Heart Timing Signal

The modulating signal $m(t)$ of the IPFM model can be retrieved from the beat event times $t_0,\ldots,t_M$ [50], using the following reformulation of (3) as the basis:

$$\int_0^{t_k} m(\tau)d\tau = kT - t_k, \quad k = 1,\ldots,M. \tag{15}$$

Clearly, the integral of $m(t)$ equals the deviation between the expected beat event time kT ("metronome time") and the beat event time t_k. This deviation serves as the definition of the irregularly sampled heart timing signal $d_{\text{HT}}(t_k)$,

$$d_{\text{HT}}(t_k) \triangleq kT - t_k, \tag{16}$$

which can be generalized to any time t by

$$d_{\text{HT}}(t) = \kappa(t)T - t = \int_0^t m(\tau)d\tau, \tag{17}$$

where the function $\kappa(t)$ is defined by

$$\kappa(t) = \frac{1}{T}\int_0^t (1+m(\tau))d\tau, \tag{18}$$

and $\kappa(t_k) = k$. Since $m(t)$ and $d_{\text{HT}}(t)$ are linearly related by an integral, an estimator of $m(t)$ is obtained by

$$\hat{m}(t) = \frac{\partial d_{\text{HT}}(t)}{\partial t}, \tag{19}$$

where 'estimator' bears no relation to statistical inference.

The computation of $d_{\text{HT}}(t_k)$ in (16) requires that the mean RR interval is estimated by $\hat{T} = (t_M - t_0)/M$. Moreover, to facilitate the differentiation in (19), the samples $d_{\text{HT}}(t_0),\ldots,d_{\text{HT}}(t_M)$ are interpolated and resampled to a fixed rate. While $d_{\text{HT}}(t)$ depends on the location of the observation interval $[t_0,t_M]$ because $d_{\text{HT}}(0) = d_{\text{HT}}(t_M) = 0$ is always satisfied, $\hat{m}(t)$ does not since this dependence is eliminated by differentiation.

For a time-varying threshold $T(t)$, the estimator $\hat{m}(t)$ is derived based on the observation that the integrand of (3) describes the instantaneous heart rate,

$$d_{\text{HR}}(t) = \frac{1+m(t)}{T(t)}. \tag{20}$$

Since $d_{\text{HR}}(t)$ is not observable, it can be approximated either by an estimate of $\kappa(t)$ in (18) obtained by interpolation of data pairs $[t_k,k]$ followed by differentiation of $\kappa(t)$ [24]. The expression in (20) can be decomposed into mean heart rate $d_{\text{mHR}}(t)$ and heart rate variability $d_{\text{HRV}}(t)$,

$$d_{\text{mHR}}(t) = \frac{1}{T(t)}, \quad d_{\text{HRV}}(t) = \frac{m(t)}{T(t)}, \tag{21}$$

where $d_{\text{mHR}}(t)$ is characterized by much lower frequencies than $d_{\text{HRV}}(t)$. Hence, $d_{\text{mHR}}(t)$ can be retrieved by lowpass filtering of $d_{\text{HR}}(t)$. Since $T(t)$ is inversely related to $d_{\text{mHR}}(t)$, the time-varying version of $d_{\text{HT}}(t_k)$ in (16) becomes

$$d_{\text{HT}}(t_k) = \frac{k}{d_{\text{mHR}}(t_k)} - t_k. \tag{22}$$

Finally, estimation of $m(t)$ is accomplished by either performing the differentiation in (19) or using the following expression which results from reorganizing (20) [79]:

$$\begin{aligned}\hat{m}(t) &= \tilde{d}_{\text{HR}}(t)\tilde{T}(t) - 1 \\ &= \frac{\tilde{d}_{\text{HR}}(t) - \tilde{d}_{\text{mHR}}(t)}{\tilde{d}_{\text{mHR}}(t)} = \frac{\tilde{d}_{\text{HRV}}(t)}{\tilde{d}_{\text{mHR}}(t)},\end{aligned} \tag{23}$$

where $\tilde{}$ indicates that the signal is obtained from the approximated $d_{\text{HR}}(t)$. Thus, $\hat{m}(t)$ is simply given by the ratio of a signal

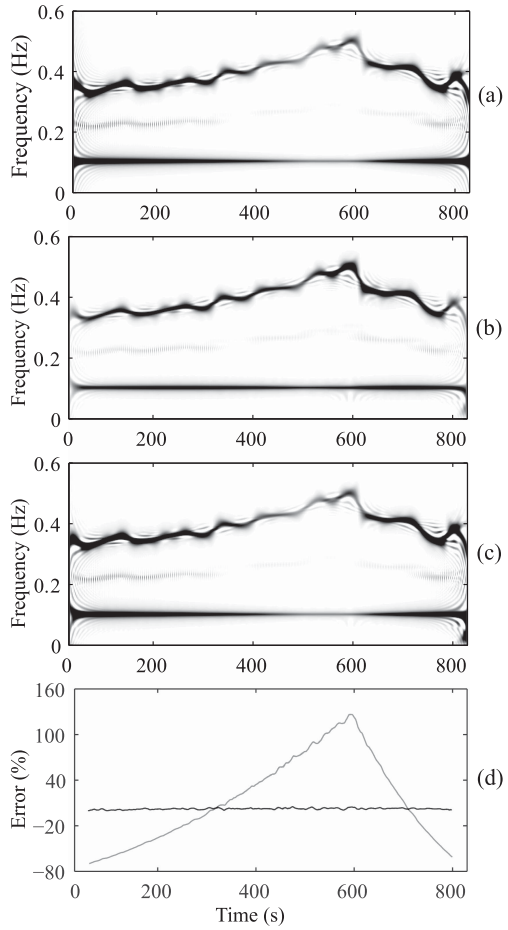

Fig. 3. Estimation of $m(t)$ under time-varying conditions. The smoothed pseudo Wigner–Ville distribution computed for (a) a simulated, two-component modulation function $m(t)$ with a constant LF component and a time-varying HF component; $\hat{m}(t)$ is obtained by equations (b) (19) and (c) (23). (d) The percentage spectral power error of the HF component obtained by (19) (grey line) and (23) (black line). The estimated signals were obtained by interpolation and resampling to 4 Hz. Reprinted from [79] with permission.

reflecting heart rate variability to a signal reflecting mean heart rate, obtained by lowpass filtering of $d_{\mathrm{IIF}}(t)$.

The importance of using (23) in time-varying conditions is illustrated by the simulation example in Fig. 3, with changes typically observed during exercise stress testing [79]. Using the smoothed pseudo Wigner–Ville distribution (SPWVD) [80] for time–frequency analysis, Fig. 3(a) displays the SPWVD of $m(t)$ dominated by an LF component held constant at 0.1 Hz and an HF component varying between 0.35 Hz and 0.5 Hz; both components have powers mimicking the variation in real data. Fig. 3(b)–(c) display the SPWVDs of $\hat{m}(t)$ obtained with (19) and (23), respectively. Comparing Fig. 3(a) and (b), it is obvious that the intensities of both components differ considerably, particularly at the onset, about 600 s, and the end of the observation interval. On the other hand, the SPWVDs displayed in Fig. 3(a) and (c) are in close agreement, thus highlighting the importance of assuming the time-varying IPFM model when analyzing time-varying data. The error made when estimating the power of the HF component is displayed in Fig. 3(d) for the two estimators: the error is essentially zero for the time-varying estimator.

Considering instead the pulse frequency modulation model, also related to the IPFM model, it can be shown that the modulating part of the interval tachogram $d_{\mathrm{IT}}(\mathrm{k})$ is influenced by the mean interevent interval $T(t)$ in a way similar to the heart timing signal [71].

B. The History-Dependent Point Process Signals

The meaning of heart rhythm representation in point process modeling is not as unequivocal as in IPFM modeling since four indices, μ_{RR}, σ_{RR}, μ_{HR}, and σ_{HR}, rather than one, $m(t)$, convey rhythm information. Of these four indices, the time-varying variant of μ_{HR} is often used for spectral analysis [77], and, therefore, it may be viewed as an equivalent to $(1+m(t))/T$. To compute these indices, estimates of the model parameters $\mathbf{a}$ and λ first need to be obtained from the observed RR intervals and then substituted into the respective defining equations.

Maximum likelihood estimation is the standard technique for finding the parameter values of a statistical model. The estimator is given by

$$[\hat{\mathbf{a}}, \hat{\lambda}] = \arg\max_{\mathbf{a},\lambda} \log p(t_0, \ldots, t_M; \mathbf{a}, \lambda), \tag{24}$$

where the joint PDF $\log p(t_0, \ldots, t_M; \mathbf{a}, \lambda)$ becomes the log-likelihood function when evaluated for the event times observed in the interval $[t_0, t_M]$. Assuming that the RR intervals $r_k = t_k - t_{k-1}$ are statistically independent, i.e., r_k is a renewal process, the joint PDF simplifies to

$$p(t_0, \ldots, t_M; \mathbf{a}, \lambda) = \prod_{k=1}^{M} p(r_k; \mathbf{a}, \lambda), \tag{25}$$

where $p(r_k; \mathbf{a}, \lambda)$ is the inverse Gaussian PDF in (9). Due to the introduction of history dependence, cf. (8), the maximization of the log-likelihood function in (24) has to be performed numerically using, e.g., the Newton–Raphson method.

Since this approach yields a description of the entire observation interval by four scalar estimates, i.e., $\hat{\mu}_{\mathrm{RR}}$, $\hat{\sigma}_{\mathrm{RR}}$, $\hat{\mu}_{\mathrm{HR}}$, and $\hat{\sigma}_{\mathrm{HR}}$, a sliding window approach was introduced to produce time-varying (local) estimates $\hat{\mu}_{\mathrm{RR}}(t)$, $\hat{\sigma}_{\mathrm{RR}}(t)$, $\hat{\mu}_{\mathrm{HR}}(t)$, and $\hat{\sigma}_{\mathrm{HR}}(t)$ based on the RR intervals in the fixed-length window $[t-\Delta t, t]$ [77]. The structure of the local log-likelihood function is essentially the same as that of the global one in (24), with the difference that the function accounts for an observation interval whose boundaries are not defined by event times. Another difference is that an exponentially decaying weighting function, defined by the parameter α, is introduced to assign more weight to the more recent RR intervals.

The goodness-of-fit of the point process model to the RR intervals can be evaluated by analyzing the conditional intensity function, specifying how the present depends on the past in a point process [81], together with a statistical test such as the Kolmogorov–Smirnov test [82]. The goodness-of-fit information is useful when trying to improve the structure of the model, but also for determining the model order p, the window length

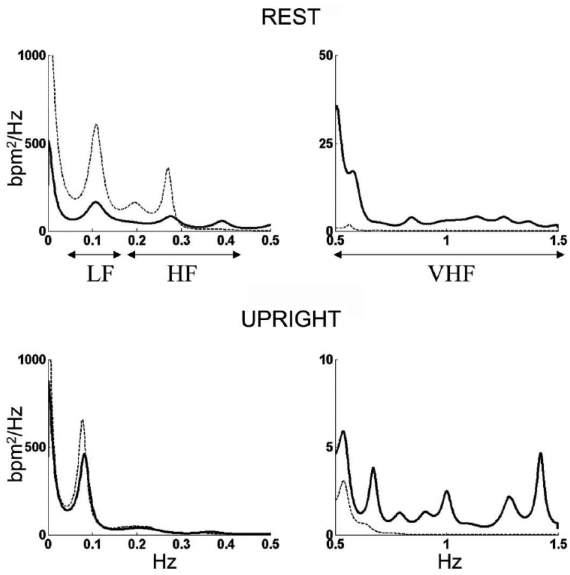

Fig. 4. Autoregressive spectral analysis of $\hat{\mu}_{\mathrm{HR}}(t)$ (solid line) during rest and upright posture, compared to the spectrum of $d_{\mathrm{IIF}}(t)$ (dashed line) resampled at a rate of 3 Hz. The upper/lower left diagrams display the power spectra for 0–0.5 Hz, whereas the upper/lower right diagrams display the power spectra for 0.5–1.5 Hz, referred to as the very high frequency (VHF) band. Reprinted from [77] with permission.

Δt, and the exponential decay α—parameters which are not part of the above-mentioned maximum likelihood estimation [77].

Adaptive filtering has also been proposed for estimating the parameters in continuous time. The filter, having a recursive structure, is defined by a set of equations resembling those defining the well-known Kalman filter [83]. It remains to be shown which of the estimation techniques is to be preferred.

Figure 4 displays the autoregressive power spectra obtained during rest and upright postures when $\hat{\mu}_{\mathrm{HR}}(t)$ and the inverse interval function $d_{\mathrm{IIF}}(t)$ is used. Clearly, the spectra are expected to differ since they are based on different rhythm representations: $d_{\mathrm{IIF}}(t)$ accounts for HRV as a whole, whereas $\hat{\mu}_{\mathrm{HR}}(t)$ and $\hat{\sigma}_{\mathrm{HR}}(t)$ account for distinctly different aspects. However, the differences can to some extent be explained by considerations of bandwidth and model order selection. Before computing the power spectrum, $d_{\mathrm{IIF}}(t)$ needs to be lowpass filtered, using a cutoff frequency well below half the mean heart rate, so that aliasing is avoided in the interpolated and resampled signal [24]. On the other hand, no such filtering was done before the power spectrum of $\hat{\mu}_{\mathrm{HR}}(t)$ was computed, and, therefore, the frequency components exceeding half the mean heart rate are aliased. Concerning model order selection, it is well-known that a larger bandwidth implies a higher model order to model the spectral peaks adequately [24]. Therefore, considering that the bandwidth of $\hat{\mu}_{\mathrm{HR}}(t)$ is much larger than that of $d_{\mathrm{IIF}}(t)$, the same model order implies lower spectral peaks using $\hat{\mu}_{\mathrm{HR}}(t)$ than for $d_{\mathrm{IIF}}(t)$.

IV. Model-Based Ectopic Beat Correction

The presence of ectopic beats perturbs the impulse pattern initiated by the sinoatrial node, thus disqualifying the RR intervals adjacent to an ectopic beat for HRV analysis. In such cases, the autonomic modulation of the sinoatrial node is temporarily lost and instead an ectopic focus initiates the next beat prematurely. The location of the ectopic focus gives rise to different types of perturbation: a beat of ventricular origin inhibits the next sinus beat so that a compensatory pause is introduced after the ectopic beat, whereas a beat of supraventricular origin or a retrograde beat discharges the sinoatrial node ahead of schedule ("resetting beat") and causes the following sinus beat to also occur ahead of schedule.

Ectopic beats must be dealt with before spectral analysis can be performed; if not, spurious frequencies will appear. Different techniques have been proposed to correct for occasional ectopic beats, whereas frequent ectopic beats perturb the rhythm to such an extent that the entire series has to be excluded from further analysis. While the majority of correction techniques do not rely on a model, but rather perform either deletion, interpolation, or filtering, see, e.g. [84], [85], [86], [87], [88], [89], [90], [91], a number of model-based techniques have been proposed, described in the following, which all originate from the IPFM model though their respective structures differ quite considerably.

Beat classification involving morphologic information is assumed to be performed before HRV analysis, providing information on whether a detected event is a normal beat, an ectopic beat, or false, e.g., a T-wave, noise, or motion artifacts; if false, the event is removed from the RR interval series.

A. Correction Based on the Lowpass Filtered Event Series

An early work on model-based correction explored the idea of replacing an ectopic beat with an imaginary normal beat whose event time deviates the least from the rhythm implied by the IPFM model [92]. Beat replacement operates under the constraint that the ectopic beat must be followed by a complete compensatory pause. Other types of ectopic beats cannot be handled, e.g., those which reset the SA node.

The lowpass filtered event series, defined by

$$d_{\mathrm{LE}}(t) = h(t) * \sum_{k=0}^{M} \delta(t - t_k), \tag{26}$$

plays an important role since it has been shown that $d_{\mathrm{LE}}(t)$ approximates $1 + m(t)$, i.e., the integrand in (2), provided that $|m(t)| \ll 1$ [24], [93]; $h(t)$ is the impulse response of an ideal lowpass filter with a cutoff frequency of $1/2T$ Hz. Consequently, as long as the event series is accounted for by the IPFM model, i.e., without any ectopic beat, the integral of $d_{\mathrm{LE}}(t)$ is approximately constant for all k since

$$T = \int_{t_{k-1}}^{t_k} (1 + m(t))dt \approx \int_{t_{k-1}}^{t_k} d_{\mathrm{LE}}(t)dt = T(t_k). \tag{27}$$

Since this integral does not hold for an event series with an ectopic beat at t_{k_e}, the replacement strategy is to find that t_{k_e} which deviates the least from the rhythm implied by the IPFM model. Accordingly, t_{k_e} relates to an imaginary normal beat instead of an ectopic beat. The replacement strategy is defined

by minimization of the variance:

$$\hat{t}_{k_e} = \arg \min_{t_{k_e-1} < t_{k_e} < t_{k_e+1}} \sum_{k=1}^{M} \left(T(t_{k_e}) - \bar{T} \right)^2, \qquad (28)$$

where $\bar{T}$ is the mean of T_k. It should be noted that $d_{\mathrm{LE}}(t)$ has to be recomputed for different values of t_{k_e}, cf. (26), and, consequently, the integral in (27) that defines $T(t_k)$.

Since this approach is constrained to only handle a premature ectopic beat followed by a complete compensatory pause, subsequent work has dealt with how to handle other types of ectopic beats.

B. Correction Based on the Heart Timing Signal

Another approach is to modify $d_{\mathrm{HT}}(t_k)$ in (16) so that normal beats following an ectopic beat at t_e ($t_{k_e} < t_e < t_{k_e+1}$) are related to a compensated time basis $(k+s)T$ instead of kT [94]; in contrast to the methods described in Sections IV-A and IV-D, t_{k_e} here represents a normal beat. As a result, correction applies also to an ectopic beat not followed by a complete compensatory pause. In this approach, the ectopic beat is not indexed by k as it is not replaced by a normal beat. Thus, the modified $d_{\mathrm{HT}}(t_k)$ is defined by

$$d_{\mathrm{HT}}(t_k) = \begin{cases} kT - t_k, & k = 1, \ldots, k_e; \\ (k+s)T - t_k, & k = k_e + 1, \ldots, M, \end{cases} \qquad (29)$$

where the unknown parameter s represents a jump in the resetting of the IPFM model.

A key step to facilitate the estimation of s is to generalize the IPFM model so that the index k is replaced by the indexing function $\kappa(t)$, which when sampled at t_k equals

$$\kappa(t_k) = \begin{cases} k, & k = 1, \ldots, k_e; \\ k + s, & k = k_e + 1, \ldots, M. \end{cases} \qquad (30)$$

Then, s can be estimated by extending $\kappa(t)$ forward in time using the event times preceding the ectopic beat, i.e., $(t_0, 0), \ldots, (t_{k_e}, k_e)$ and extending $\kappa(t) + s$ backward in time using the event times following the ectopic beat $(t_{k_e+1}, k_e + 1)$, $\ldots, (t_M, M)$ so that the two extended functions overlap. The forward extension introduces a new event time $\hat{t}^f_{k_e+1}$ under the assumption that the sinus rhythm continues after t_{k_e}, and, similarly, the backward extension introduces a new time $\hat{t}^b_{k_e}$ ($< \hat{t}^f_{k_e+1}$) under the assumption that the sinus rhythm precedes t_{k_e+1}; for details on extension by extrapolation, see [94]. Using the least squares criterion, the estimator of s is

$$\hat{s} = \frac{1}{\hat{t}^f_{k_e+1} - \hat{t}^b_{k_e}} \int_{\hat{t}^b_{k_e}}^{\hat{t}^f_{k_e+1}} \left(\hat{\kappa}^f(t) - \hat{\kappa}^b(t) \right) dt, \qquad (31)$$

i.e., the area enclosed by the forward and backward extended functions $\hat{\kappa}^f(t)$ and $\hat{\kappa}^b(t)$ within the overlap, normalized by the duration of the overlap, see Fig. 5. A value of s close to one indicates that the event at t_e is likely a premature ectopic beat followed by a compensatory pause, whereas a value close to zero indicates that the event is likely an artifact.

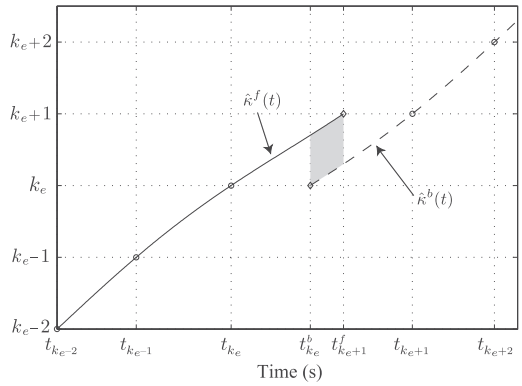

Fig. 5. Ectopic beat correction based on $d_{\mathrm{HT}}(t_k)$. Forward extension of the indexing function $\hat{\kappa}^f(t)$ using the event times $(t_0, 0), \ldots, (t_{k_e}, k_e)$ and backward extension of $\hat{\kappa}^b(t)$ using the event times $(t_{k_e+1}, k_e + 1), \ldots, (t_M, M)$; $\hat{\kappa}^f(t)$ and $\hat{\kappa}^b(t)$ are extended until they overlap in time. The least squares estimator of s computes the shaded area, normalized by the duration of the overlap, cf. (31).

Before the modified heart timing signal can be computed, the estimator of T has to be modified so that it accounts for $\hat{s}$,

$$\hat{T} = \frac{t_M - t_0}{M + \hat{s}}. \qquad (32)$$

C. Simplified Correction Based on the Heart Timing Signal

Because of the extrapolation required to compute (31), the correction based on $d_{\mathrm{HT}}(t_k)$ is computationally rather demanding. Therefore, a simplified correction was developed building on the observation that an ectopic beat shifts the event times of the following normal beats by a certain time δ [95]. Then, an alternative formulation of $d_{\mathrm{HT}}(t_k)$ is given by

$$d_{\mathrm{HT}}(t_k) = \begin{cases} kT - t_k, & k = 1, \ldots, k_e; \\ kT - t_k + \delta, & k = k_e + 1, \ldots, M. \end{cases} \qquad (33)$$

The time shift δ can be derived by studying the interval from t_{k_e} to $t_{k_e+1} - \delta$, where the latter event time relates to a normal beat had an ectopic beat not occurred. Then, the integral defining the IPFM model for the normal beats at t_{k_e} and t_{k_e+1} can be decomposed as follows:

$$\int_{t_{k_e}}^{t_{k_e+1}} (1 + m(\tau)) d\tau = \underbrace{\int_{t_{k_e}}^{t^f_{k_e+1} = t_{k_e+1} - \delta} (1 + m(\tau)) d\tau}_{= T} + \int_{t_{k_e+1} - \delta}^{t_{k_e+1}} (1 + m(\tau)) d\tau,$$

where evaluation of the first integral yields the following expression of δ:

$$\delta = t_{k_e+1} - t_{k_e} - T + \int_{t_{k_e}}^{t_{k_e+1} - \delta} m(\tau) d\tau. \qquad (34)$$

To make this expression practicable, $m(t)$ can be approximated by a constant during the ectopic beat (defining the first-order estimator of δ), by a linear change during the ectopic beat

(defining the second-order estimator of δ), and so on. The general N-th order estimator of δ is given by [95]

$$\hat{\delta}_N = \sum_{l=0}^{N+1} (-1)^l \binom{N+1}{l} t_{k_e+1-l}, \quad N = 1, 2, \ldots \tag{35}$$

In analogy with (32), the estimator of T is modified to account for $\hat{\delta}_N$, given by

$$\hat{T} = \frac{t_M - t_0 - \hat{\delta}_N}{M}. \tag{36}$$

By comparing the results obtained by spectral analysis, the power of the LF and HF bands were found to be almost identical for the corrections based on (29) and (33) using $\hat{\delta}_1$, with the difference that the latter type of correction is computationally much more efficient [95].

D. Correction Based on Point Process Modeling

The history-dependent point process model has been successfully adopted for ectopic beat correction by exploring the assumption that RR intervals in sinus rhythm can be modeled by a time-varying inverse Gaussian PDF [96]. Similar to the correction method described in Sec. IV-A, an ectopic beat is replaced by an imaginary normal beat, but with the difference that the event time is determined by assessing to what extent the event time fits the model. Again, beat replacement operates under the constraint that the ectopic beat must be followed by a complete compensatory pause.

The starting point of the correction is the two PDFs describing the RR intervals adjacent to the ectopic beat at t_{k_e}. By maximizing the product of these two PDFs,

$$\hat{t}_{k_e} = \arg \max_{t_{k_e-1} < \tau < t_{k_e+1}} p(\tau - t_{k_e-1}; \hat{\mu}(\mathcal{H}_{k_e-1}, \boldsymbol{a}_{k_e-1}), \lambda_{k_e-1}) \cdot p(t_{k_e+1} - \tau; \hat{\mu}(\mathcal{H}_{k_e}(\tau), \boldsymbol{a}_{k_e}), \lambda_{k_e}), \tag{37}$$

the most probable event time $\hat{t}_{k_e}$ of an imaginary normal beat is determined, thus replacing t_{k_e} in the corrected series of event times. The mean of the PDF of the RR interval preceding the ectopic beat is given by

$$\hat{\mu}(\mathcal{H}_{k_e-1}, \boldsymbol{a}_{k_e-1}) = \hat{a}_{0,k_e-1} + \sum_{i=1}^{p} \hat{a}_{i,k_e-1}(t_{k_e-i} - t_{k_e-1-i}), \tag{38}$$

where the regression parameters a_{i,k_e-1} are estimated using the p event times preceding the ectopic beat, i.e., $t_{k_e-p}, \ldots, t_{k_e-1}$. The mean of the PDF of the RR interval following the ectopic beat accounts for that the event time τ is shifted and given by

$$\hat{\mu}(\mathcal{H}_{k_e}(\tau), \boldsymbol{a}_{k_e}) = \hat{a}_{0,k_e} + \hat{a}_{1,k_e}(\tau - t_{k_e-1}) + \sum_{i=2}^{p} \hat{a}_{i,k_e}(t_{k_e-i+1} - t_{k_e-i}). \tag{39}$$

The regression parameters a_{i,k_e} are estimated from a slightly different series of event times which includes the event time τ subject to estimation, i.e., $t_{k_e-p+1}, \ldots, t_{k_e-1}, \tau$. The shape parameters λ_{k_e-1} and λ_{k_e} in (37) can be estimated using the event time series $\mathcal{H}_{k_e-1}$ and $\mathcal{H}_{k_e}(\tau)$, respectively. Another, simpler approach is to first estimate λ_{k_e-1} and then setting $\hat{\lambda}_{k_e} = \hat{\lambda}_{k_e-1}$ [96]. The maximization in (37) is performed numerically using, e.g., the Newton–Raphson algorithm.

Before the corrected series can be accepted, the probability describing how well the model fits several RR intervals preceding and following the ectopic beat at t_{k_e} has to be evaluated. The corrected series is accepted only if the probability exceeds, with a certain margin, the probability associated with the original, uncorrected series.

V. Time–Frequency Analysis of HRV in Time-Varying Conditions

The standard, fixed definitions of the HRV frequency bands are inappropriate in conditions when the respiratory frequency varies considerably over time, e.g., during exercise stress testing. This issue may be addressed by redefining the HF band on the basis of respiratory frequency and mean heart rate. Another issue arising in time-varying conditions relates to spurious, aliased spectral components sometimes observed during exercise stress testing. While time–frequency analysis serves as the backbone to handle these issues, additional methods are needed to ensure adequate interpretation, most of them heuristic in nature and therefore without relation to the previously described models.

A. Respiration and HF Band Redefinition

The power of the HF band (0.15–0.4 Hz) is considered a measure of efferent vagal activity mainly due to respiratory activity, a consideration that builds on the assumption that the respiratory frequency is contained in this band. However, the use of a fixed HF band is inadequate, e.g., in situations of physical activity and autonomic provocation and in children and pregnant women, when the respiratory frequency very well can exceed 0.4 Hz. Conversely, the respiratory frequency may subceed 0.15 Hz during sleep and relaxation, clearly leading to inadequate measurements when using fixed LF and HF bands. This problem may be addressed using the signal decomposition techniques described in Section VII.

Several approaches have been proposed to handle the drawbacks of a fixed HF band, all having in common that a respiratory signal $r(t)$, whether measured from a dedicated sensor or ECG-derived, is used to redefine the HF band. Irrespective of approach, the HF band must be upper bounded by half the mean heart rate due to the sampling theorem. In those extreme occasions when the respiratory frequency exceeds half the mean heart rate, aliasing components will appear at frequencies below half the mean heart rate [8]; Section V-B provides insight into how to mitigate this problem.

An early approach to redefining the standard HF band was to simply increase the upper limit to 0.60 Hz to ensure that the respiratory frequency always remained within the band [97]. However, a broadened HF band increases the risk of including spurious spectral peaks which in turn leads to HF power measurements suggesting increased parasympathetic activity. Another early approach was to center the HF band to a fixed respiratory frequency, determined either by a metronome [98] or derived from the power spectrum $S_d(F)$ of $d(t)$ [99], [100]. Once determined, the HF band was held fixed throughout the

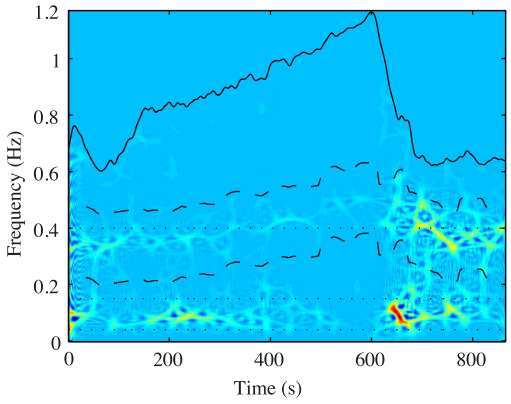

Fig. 6. The SPWVD of an HRV signal obtained during exercise stress testing (lasting until 600 s) and recovery, highlighting how the HF band is redefined based on the respiratory frequency. Half the mean heart rate is plotted with a solid black line, the respiratory-related, time-varying limits of the HF band with dashed lines, and the standard, fixed limits of the LF and HF bands with dotted lines.

recording. However, deriving the respiratory frequency from $S_d(F)$ is highly susceptible to errors due to phantom peaks [32], broadband respiration, and reduced respiratory sinus arrhythmia. Therefore, modern methods for ECG-derived respiration explore beat morphology which is much more robust.

In more recent studies, the HF band $\Omega_{\text{HF}}(t)$ is redefined on the basis of a time-varying respiratory frequency $F_r(t)$ and related limits defined by $\Delta_l(t)$ and $\Delta_u(t)$,

$$\Omega_{\text{HF}}(t) \equiv [F_r(t) - \Delta_l(t), F_r(t) + \Delta_u(t)]\,. \tag{40}$$

Based on the time–frequency distribution of an airflow signal, $F_r(t)$ was determined by finding the location of the largest peak of each time slice, which, together with the assumption of a fixed bandwidth, i.e., $\Delta_l(t) = \Delta_u(t) = \Delta$, defined $\Omega_{\text{HF}}(t)$ [101], [102]. Based on the scalogram of a plethysmographic signal, $F_r(t)$ was also determined by finding the location of the largest peak of each time slice, whereas $\Delta_l(t)$ and $\Delta_u(t)$ were determined by finding the locations of the two minima immediately surrounding the largest peak [103]. Unfortunately, such a definition tends to produce an $\Omega_{\text{HF}}(t)$ which varies considerably from slice to slice, thus warranting a more robust method. This may be achieved by computing the sample Pearson correlation coefficient between $S_r(F)$ and $S_d(F)$ in a small interval around $F_r(t)$ (determined from the location of the largest peak in $S_r(F)$), then increasing the interval limits until the correlation coefficient falls below a certain threshold when the limits are designated as $\Omega_{\text{HF}}(t)$ [104]. While the method was originally developed for stationary conditions, it can be easily extended to nonstationary conditions.

Preventive measures must be taken to avoid that the redefined HF band overlaps with the LF band, e.g., by requiring that $F_r(t) - \Delta_l(t) > 0.15$ Hz [79], [105], or by simply setting the upper limit of the LF band to $F_r(t) - \Delta_l(t)$ [104]. The preventive measures refer to situations when the respiratory frequency $F_r(t)$ is low, then resulting in a lower limit of the HF band which is below 0.15 Hz.

Figure 6 illustrates how the spectral content of an HRV signal, obtained during exercise stress testing and recovery, varies over time. The respiratory frequency exceeds the upper limit of the standard, fixed HF band from about 400 s to 700 s, and, consequently, tracking the power of this HF band yields an inaccurate description of parasympathetic activity. By redefining the HF band based on respiratory frequency [101], [102], the power of the redefined HF band is found to decrease during exercise, thus reflecting parasympathetic withdrawal, accompanied by an increase during recovery.

Rather than explicitly relating the HF band limits to $F_r(t)$ as in (40), $\Omega_{\text{HF}}(t)$ may be based on the local coupling between $d(t)$ and $r(t)$. While $F_r(t)$ may still be used, it plays a subordinate role in indicating the region of interest for subsequent spectral analysis. One statistical approach to determining $\Omega_{\text{HF}}(t)$ is based on time–frequency coherence which measures the strength of the local coupling between $d(t)$ and $r(t)$, defined by [106]

$$\gamma_{dr}(t,F) = \frac{|S_{dr}(t,F)|}{\sqrt{S_d(t,F)S_r(t,F)}}, \tag{41}$$

where $S_{dr}(t,F)$ denotes the time-dependent cross-spectrum between $d(t)$ and $r(t)$, and $S_d(t,F)$ and $S_r(t,F)$ denote the time-dependent power spectra of $d(t)$ and $r(t)$, respectively. Since this measure is well suited for finding regions in the time–frequency domain where $d(t)$ and $r(t)$ exhibit similar instantaneous frequencies, it has been proposed for redefining the HF band [107]. The computation of $S_{dr}(t,F), S_d(t,F)$, and $S_r(t,F)$ needs to be made with caution to ensure that $\gamma_{dr}(t,F)$ is bounded between 0 and 1. This applies particularly to the kernel function chosen to weight the ambiguity function (reflecting the uncertainty in time and frequency) to suppress undesired cross-terms [15], [107]. To find regions of coherence in $\gamma_{dr}(t,F)$, hypothesis testing is performed on a point-by-point basis by comparing $\gamma_{dr}(t,F)$ to a threshold $\gamma_{\text{TH}}(t,F;\alpha)$,

$$\Omega_{\text{HF}}(t) \equiv \{\gamma_{dr}(r,F) > \gamma_{\text{TH}}(t,F;\alpha)\}. \tag{42}$$

The null hypothesis H_0, stating that $d(t)$ and $r(t)$ are uncorrelated at a certain point in the time–frequency domain, is rejected at the significance level α whenever the inequality in (42) is fulfilled. For this particular significance level, the threshold $\gamma_{\text{TH}}(t,F;\alpha)$ is determined by computing $\gamma_{dr}(t,F)$ for several realizations of surrogate signals without local coupling; the surrogate signals can be white noise or have properties similar to the original signals [108]. Using this approach, the resulting HF band may contain discontinuities ("gaps") in time as well as in frequency.

B. Spurious Spectral Components During Exercise

During exercise stress testing, performed either by pedaling a bicycle ergometer or running on a treadmill, the interpretation of the HRV spectrum is complicated by the appearance of a spurious locomotor-related component centered at the pedaling or running stride frequency $F_l(t)$. This component is observed during a maximal graded bicycle ergometer stress test, particularly at higher workloads when the locomotor–heart rate coupling (synchronization) is accentuated [109]. The coupling may

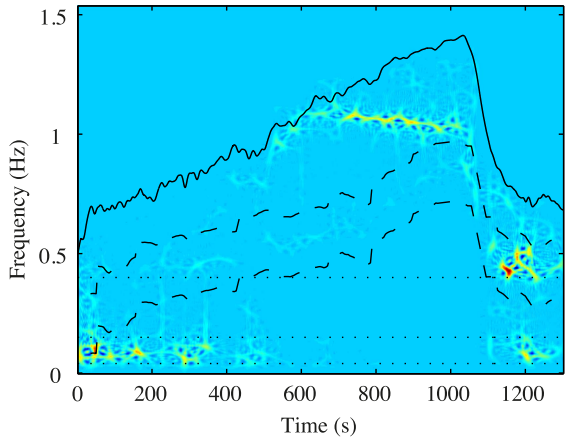

Fig. 7. The SPWVD of an HRV signal obtained during exercise stress testing (lasting until just after 1000 s) and recovery, highlighting the component due to pedaling at 60 revolutions per minute, i.e., $F_l(t) = 1$ Hz, visible from about 600 to 1000 s when below half the mean heart rate $F_{\mathrm{mHR}}(t)$ (solid line). The respiratory-related, time-varying limits of the HF band are indicated with dashed lines, and the standard, fixed limits of the LF and HF bands with dotted lines. No aliased component is present when $F_l(t)$ is below $F_{\mathrm{mHR}}(t)/2$.

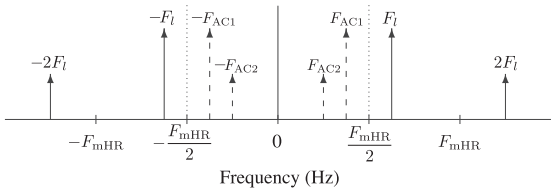

Fig. 8. Schematic illustration of the aliasing introduced by the pedaling/stride frequency F_l and its harmonic at $2F_l$; the aliased components appear at F_{AC1} and F_{AC2}. For clarity, time-dependence is omitted.

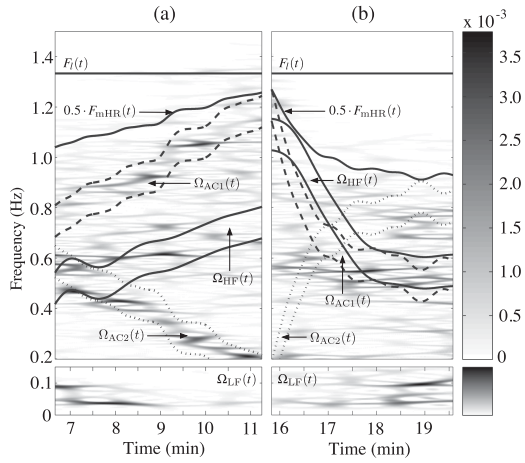

Fig. 9. The SPWVD of an HRV signal obtained during exercise stress testing when pedaling is performed (a) with increasing workload and (b) without workload during recovery, illustrating how the frequency bands, whether related to autonomic function or aliasing, change over time. During certain periods, $\Omega_{\mathrm{HF}}(t)$ (solid lines) overlap with $\Omega_{\mathrm{AC1}}(t)$ (dashed lines) and/or $\Omega_{\mathrm{AC2}}(t)$ (dotted lines).

be explained as a consequence of heart rate entrainment by locomotor rhythms due to interaction [110]. Another explanation is related to the projection of the cardiac electrical vector onto different leads: at higher workloads, the direction of the vector is increasingly coupled to $F_l(t)$ causing the QRS morphology to change in a rhythmical fashion [111]. As a result, the event times produced by the QRS detector exhibit slight jittering which in the HRV spectrum is manifested as a component at $F_l(t)$. The presence of this component is illustrated by Fig. 7 where the time–frequency distribution of an HRV signal, obtained during exercise stress testing and recovery, is displayed.

When the spurious component at $F_l(t)$ exceeds half the mean heart rate $F_{\mathrm{mHR}}(t)$, an aliased component is introduced in the HRV spectrum that may overlap with the LF or the HF band [112]. When the pedaling/stride frequency varies during exercise stress testing, additional aliased components may be introduced which, together with the autonomic HRV components of interest, form a pattern difficult to disentangle.

Figure 8 illustrates schematically how aliasing is introduced by $F_l(t)$ and its harmonic at $2F_l(t)$ when $F_l(t) > F_{\mathrm{mHR}}(t)/2$; the two aliased components appear at the frequencies $F_{\mathrm{AC1}}(t)$ and $F_{\mathrm{AC2}}(t)$. Figure 9 shows the time–frequency distribution of an HRV signal of a subject running on a treadmill at fixed frequency. The HF band $\Omega_{\mathrm{HF}}(t)$ and the bands related to the aliased components, denoted $\Omega_{\mathrm{AC1}}(t)$ and $\Omega_{\mathrm{AC2}}(t)$, are superimposed on the time–frequency distribution. The aliasing bands are centered at $F_{\mathrm{mHR}}(t) - F_l(t)$ and $-F_{\mathrm{mHR}}(t) + 2F_l(t)$, in both cases assumed to have a bandwidth of 0.125 Hz.

When $F_l(t)$ subceeds $F_{\mathrm{mHR}}(t)/2$, no aliased component is present. While $F_l(t)$ itself may cause problems, it is typically much higher than $F_r(t)$, and, therefore, its influence on the HF band is negligible unless an extended HF band is used.

When information on pedaling/stride frequency and mean heart rate indicates the presence of one or several aliased components, a correction technique can be applied when computing the HF power [111]. The correction is activated as soon as $\Omega_{\mathrm{A}}(t)$, $\mathrm{A} \in \{\mathrm{AC1}, \mathrm{AC2}, \ldots\}$, overlaps with $\Omega_{\mathrm{HF}}(t)$, where 'ACn' stands for the n:th aliased component. The degree of overlap is defined by

$$o_{\mathrm{HF,A}}(t) = \frac{\Omega_{\mathrm{HF,A}}(t)}{\Omega_{\mathrm{A}}(t)}, \quad 0 \le o_{\mathrm{HF,A}}(t) \le 1, \tag{43}$$

where $\Omega_{\mathrm{HF,A}}(t)$ is the bandwidth of the overlap; thus, $o_{\mathrm{HF,A}}(t) = 0$ indicates no overlap. The correction depends on the relative power of $\Omega_{\mathrm{HF}}(t)$ and $\Omega_{\mathrm{A}}(t)$, meaning that more correction is applied when the aliased components become more dominant. The relative power is defined by

$$\alpha_{\mathrm{HF,A}}(t) = \frac{P_{\mathrm{A}}(t)}{P_{\mathrm{HF}}(t) + P_{\mathrm{A}}(t)}, \quad 0 \le \alpha_{\mathrm{HF,A}}(t) < 1. \tag{44}$$

To ensure that $\alpha_{\mathrm{HF,A}}(t)$ is a smooth function, a running average $\bar{\alpha}_{\mathrm{HF,A}}(t)$ is used, updated as long as $o_{\mathrm{HF,A}}(t) = 0$, but extrapolated by holding fixed the most recent update of $\bar{\alpha}_{\mathrm{HF,A}}(t)$ whenever $o_{\mathrm{HF,A}}(t) > 0$. The corrected HF power $\tilde{P}_{\mathrm{HF}}(t)$ is obtained by subtracting $P_{\mathrm{A}}(t)$, scaled by $o_{\mathrm{HF,A}}(t)$ and $\bar{\alpha}_{\mathrm{HF,A}}(t)$, from the original HF power $P_{\mathrm{HF}}(t)$. For the case with two aliased components, $\tilde{P}_{\mathrm{HF}}(t)$ is given by

$$\tilde{P}_{\mathrm{HF}}(t) = P_{\mathrm{HF}}(t) - o_{\mathrm{HF,AC1}}(t)\bar{\alpha}_{\mathrm{HF,AC1}}(t)P_{\mathrm{AC1}}(t)$$

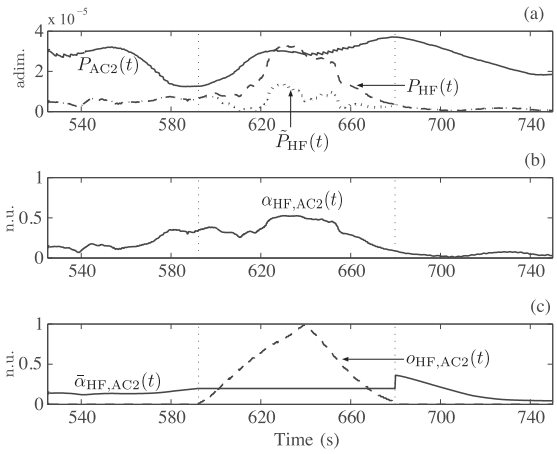

Fig. 10. Illustration of HF power correction using (45). (a) The uncorrected HF power $P_{\mathrm{HF}}(t)$ (dashed line), the power of the aliased component $P_{\mathrm{AC2}}(t)$ (solid line), and the corrected HF power $\tilde{P}_{\mathrm{HF}}(t)$ (dotted line), (b) the relative power $\alpha_{\mathrm{HF,AC2}}(t)$, and (c) the degree of overlap $o_{\mathrm{HF,AC2}}(t)$ (dashed line) and the running average $\bar{\alpha}_{\mathrm{HF,AC2}}(t)$ (solid line). The vertical dashed lines indicate onset and end of the overlap during which $\bar{\alpha}_{\mathrm{HF,AC2}}(t)$ is held fixed.

$$- o_{\mathrm{HF,AC2}}(t)\bar{\alpha}_{\mathrm{HF,AC2}}(t)P_{\mathrm{AC2}}(t). \tag{45}$$

By holding fixed the most recent update of $\bar{\alpha}_{\mathrm{HF,A}}(t)$ whenever $o_{\mathrm{HF,A}}(t) > 0$, the HRV signal is implicitly assumed to be short-term stationary during the overlap period.

Figure 10 illustrates the correction technique for a situation in which aliasing caused by $F_l(t)$ appears during a limited time period, leading to overestimation of $P_{\mathrm{HF}}(t)$. Following the correction in (45), $\tilde{P}_{\mathrm{HF}}(t)$ decreases to values similar to those observed before and after the aliasing period.

VI. Time–Frequency Based Parameter Estimation Guided by Respiration

Rather than redefining the standard HF band to account for respiration, a model-based approach to inferring information on the LF and HF components may constitute a better alternative, especially when respiration is considered. Such an approach could then output time-varying estimates of the frequency and the power of each component. A signal-plus-noise model has been proposed with a structure particularly suitable for analysis of data recorded during exercise stress testing [102]. The model is based on the assumption that the analytic HRV signal $d_A(n)$ of the general, discrete-time HRV signal $d(n)$, obtained after interpolation and resampling at rate F_s, is composed of two complex exponentials, i.e., sinusoids, accounting for the dominant frequencies of the LF and HF bands [102], [113],

$$d_A(n) = A_{\mathrm{LF}}e^{j\omega_{\mathrm{LF}}n} + A_{\mathrm{HF}}e^{j\omega_{\mathrm{HF}}(n)n} + v_A(n), \tag{46}$$

where A_{LF} and A_{HF} are amplitudes and $\omega_{\mathrm{LF}} = 2\pi f_{\mathrm{LF}}$ and $\omega_{\mathrm{HF}}(n) = 2\pi f_{\mathrm{HF}}(n)$ are discrete-time frequencies. The exercise-induced changes in respiratory frequency are modeled by $f_{\mathrm{HF}}(n) = 2\alpha n + \beta$, i.e., increasing linearly with workload until peak exercise and then decreasing linearly during recovery; the variation in respiratory frequency is defined by 2α [114], [115]. The analytic noise $v_A(n)$ is assumed to be white, accounting for QRS jitter and modeling inaccuracies.

Reformulating the model in terms of autocorrelation conditions the model for nonparametric time–frequency analysis, with windowing as an important ingredient. Assuming a rectangular window for time smoothing, defined by the width $2N-1$, and an exponential window for frequency smoothing, defined by the decay γ, the instantaneous autocorrelation function of $d_A(n)$ is given by [102]

$$r_d(n,k) = e^{-\gamma|k|}\left(|A_{\mathrm{LF}}|^2 e^{j\omega_{\mathrm{LF}}2k} + |A_{\mathrm{HF}}|^2 u(k) e^{j\omega_{\mathrm{HF}}(n)2k}\right) + \text{cross-term} + r_v(n,k), \tag{47}$$

where

$$u(k) = \frac{1}{2N-1}\frac{\sin(2\pi 2\alpha(2N-1)k)}{\sin(2\pi 2\alpha k)}.$$

Thus, due to time smoothing, the amplitude and bandwidth of the HF component become dependent on α and N. By proper selection of N, however, the cross-term can be reduced.

Then, based on (47), a general model is given by

$$r_d(n,k) = \sum_{i=1}^{I(n)} C_i(n) e^{\xi_i(n)k + j\omega_i(n)k} + w(n,k), \tag{48}$$

where $C_i(n)$ is an amplitude, $\xi_i(n)$ a damping factor, and $w(n,k)$ accounts for $r_v(n,k)$ and the cross-term. The number of components $I(n)$ can change over time to reflect the presence of multiple HRV-related components in the LF and HF bands as well as the pedaling component.

In the absence of noise, $C_i(n)$, $\xi_i(n)$, and $\omega_i(n)$ can be estimated using a suboptimal least squares technique in which the zeros of the L-th order prediction error filter

$$B_n(z) = 1 + b(n,1)z^{-1} + \cdots + b(n,L)z^{-L}$$

are located at $z_i(n) = e^{(\xi_i(n) + j\omega_i(n))k}$, $i = 1, \ldots, L$, where L can simply be set to the rank of $\mathbf{R}_d(n)$ [102]. The coefficients $b(n,i)$, forming the column vector $\mathbf{b}(n)$, are obtained by the linear prediction equation $\mathbf{R}_d(n)\mathbf{b}(n) = \mathbf{r}_d(n)$, where $\mathbf{R}_d(n)$ is the sample autocorrelation matrix and $\mathbf{r}_d(n)$ the sample autocorrelation vector, both computed from the observed signal $d_A(n)$. Then, for each $z_i(n)$, the related frequency and damping factor are obtained by $\hat{\omega}_i(n) = \mathrm{Im}(\ln z_i(n))$ and $\hat{\xi}_i(n) = \mathrm{Re}(\ln z_i(n))$, respectively, whereas $\hat{C}_i(n)$ is obtained using a least squares approach to solving the linear system of equations that results from inserting $\hat{\xi}_i(n)$ and $\hat{\omega}_i(n)$ in (48). The power and frequency of a component are given by

$$\hat{P}_i(n) = \frac{|\hat{C}_i(n)|}{\sqrt{2}}, \quad \hat{F}_i(n) = \frac{1}{2}\frac{\hat{\omega}_i(n)}{2\pi}F_s, \tag{49}$$

where F_s is the sampling rate of the HRV signal.

Respiratory information is introduced by forcing the HF component $z_{\mathrm{HF}}(n)$ to $\hat{\omega}_{\mathrm{HF}}(n) = 2\pi f_r(n)$ and $\hat{\xi}_{\mathrm{HF}}(n)$ to a function of the rate of variation in $f_r(n)$, given by the time-varying estimator $2\hat{\alpha}(n) = f_r(n) - f_r(n-1)$ [102]; $d(n)$ and $f_r(n)$ are assumed to be sampled at the same rate. To account for the assumption that $z_{\mathrm{HF}}(n)$ is known and the presence of noise, the following

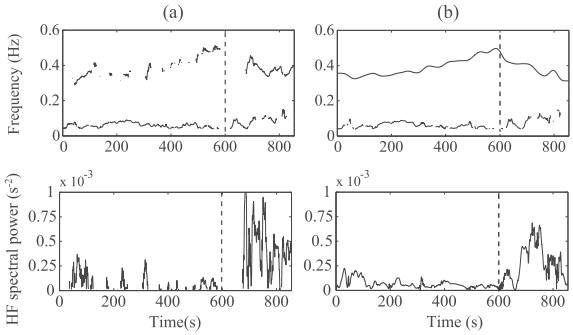

Fig. 11. The frequencies $\hat{f}_{\mathrm{LF}}(n)$ and $\hat{f}_{\mathrm{HF}}(n)$ (top row, plotted after multiplication with F_s to produce natural frequencies) and $\hat{P}_{\mathrm{HF}}(n)$ (bottom row) computed for $z_{\mathrm{HF}}(n)$ determined (a) without and (b) with use of $f_r(n)$. An extended HF band from 0.15 Hz to half the mean heart rate is assumed. Peak exercise is marked with a dashed line.

constrained least squares criterion should be minimized with respect to $\mathbf{b}(n)$:

$$J(n) = \|\mathbf{R}_d(n)\mathbf{b}(n) - \mathbf{r}_d(n)\|^2 + \lambda(\mathbf{b}^T(n)\mathbf{z}_{\mathrm{HF}}(n) + 1), \tag{50}$$

where $\mathbf{z}_{\mathrm{HF}}(n) = [z_{\mathrm{HF}}^{-1}(n), z_{\mathrm{HF}}^{-2}(n), \ldots, z_{\mathrm{HF}}^{-P}(n)]^T$ and λ is a Lagrangian multiplier. The LF component $z_{\mathrm{LF}}(n)$ is identified as the frequency $\hat{\omega}_i$ with the largest power in the LF band.

Nonparametric time–frequency analysis suffers from a time-varying frequency resolution and an unwanted time-varying amplitude term that influence the HF power estimate. However, using the time-variant rectangular window length $2N(n) - 1 = \kappa/2\hat{\alpha}(n)$, where κ is a constant, the frequency resolution becomes time-invariant. Moreover, the unwanted influence on the HF power estimate can be avoided using the following time-varying window:

$$g(n, l) = \frac{2\rho(n)}{\rho^2(n) + (2\pi l)^2},$$

where $\rho(n) = \eta/(4|\hat{\alpha}(n)|)$ and η is a constant.

Fig. 11 displays the dominant frequencies $\hat{f}_{\mathrm{LF}}(n)$ and $\hat{f}_{\mathrm{HF}}(n)$ and the power of the HF component $\hat{P}_{\mathrm{HF}}(n)$ for an HRV signal obtained during exercise stress testing. The parameters were estimated both without and with inclusion of $f_r(n)$, using unconstrained and constrained least squares estimation, respectively. Clearly, the inclusion of $f_r(n)$, defined at all times, results in lower variability in $\hat{f}_{\mathrm{HF}}(n)$ and, as a result, $\hat{P}_{\mathrm{HF}}(n)$ becomes smoother.

Even if this approach accounts for respiration, it can still be influenced by spurious components when the spectral bands overlap. If so, the correction in (45) should be considered.

VII. Signal Decomposition Guided by Respiration

In certain situations, decomposition of the HRV signal is warranted so that the respiration-related fluctuations are removed from the HRV signal so that, in turn, the signals both related and unrelated to respiration can be analyzed. For example, it has been shown that the effects of mental stress are better reflected in HRV indices derived from the decomposed HRV signal than from the original signal [116], [117]. Another situation calling for decomposition is when the LF and HF bands overlap, ultimately leading to entrainment when the two components merge into one. Such overlapping occurs during, e.g., rosary prayer and yoga [118] and wakefulness, slow-wave and REM sleep [119]. If not handled properly through decomposition, the power of the LF band will be significantly overestimated [105].

The methods described in this section focus on the following decomposition of the general, discrete-time HRV signal $d(n)$:

$$d(n) = d_r(n) + d_{ur}(n), \quad n = 0, \ldots, N-1, \tag{51}$$

where $d_r(n)$ accounts for respiratory influence on the heart rate and $d_{ur}(n)$ is the residual signal. The decomposition is usually done in two steps: first the signal with respiration-related fluctuations $\hat{d}_r(n; r(n))$ is estimated and then the residual signal is computed,

$$\hat{d}_{ur}(n) = d(n) - \hat{d}_r(n; r(n)), \tag{52}$$

where the respiratory signal $r(n)$ is needed to find $\hat{d}_r(n; r(n))$ as indicated by the functional dependence. Neither $d_r(n)$ nor $d_{ur}(n)$ have to be described by a mathematical model to be useful for decomposition.

In the following, $d(n)$ and $r(n)$ are assumed to be mean-corrected and $r(n)$ bandpass filtered so that frequencies outside the interval defined by the lower limit of the LF band and the upper limit of the HF band are suppressed.

A. Linear Filtering

A popular approach to decomposition builds on the assumption that $d_r(n)$ is related to $r(n)$ through a p-th order, linear, time-invariant filter with impulse response $h(n)$ [116], [117], [120]. With matrix representation, the decomposition can be expressed as

$$\mathbf{d} = \mathbf{R}_1\mathbf{h} + \mathbf{d}_{ur}, \tag{53}$$

where

$$\mathbf{R}_1 = \begin{bmatrix} r(p) & r(p-1) & \cdots & r(0) \\ r(p+1) & r(p) & \cdots & r(1) \\ \vdots & \vdots & \ddots & \vdots \\ r(N-1) & r(N-2) & \cdots & r(N-1-p) \end{bmatrix} \tag{54}$$

is a convolution matrix and

$$\mathbf{h} = \begin{bmatrix} h(0) & h(1) & \cdots & h(p) \end{bmatrix}^T,$$

$$\mathbf{d}_{ur} = \begin{bmatrix} d_{ur}(p) & d_{ur}(p+1) & \cdots & d_{ur}(N-1) \end{bmatrix}^T,$$

$$\mathbf{d} = \begin{bmatrix} d(p) & d(p+1) & \cdots & d(N-1) \end{bmatrix}^T.$$

The filter order p may be chosen using an information criterion such as Akaike's, however, the filter order should also account for a sufficiently low respiratory frequency [121].

The optimal least squares filter coefficients $\mathbf{h}$ are obtained by minimizing $\|\mathbf{d}_{ur}\|^2 = \|\mathbf{d} - \mathbf{R}_1\mathbf{h}\|^2$, resulting in the well-known estimator [122]

$$\hat{\mathbf{h}} = (\mathbf{R}_1^T\mathbf{R}_1)^{-1}\mathbf{R}_1^T\mathbf{d}. \tag{55}$$

The respiration-related HRV signal is obtained by the orthogonal projection

$$\hat{\mathbf{d}}_r = \mathbf{R}_1\hat{\mathbf{h}} = \mathbf{R}_1(\mathbf{R}_1^T\mathbf{R}_1)^{-1}\mathbf{R}_1^T\mathbf{d}, \tag{56}$$

where $\mathbf{P}_1 = \mathbf{R}_1(\mathbf{R}_1^T\mathbf{R}_1)^{-1}\mathbf{R}_1^T$ is a projection matrix. Thus, the residual signal is obtained by

$$\hat{\mathbf{d}}_{ur} = \mathbf{d} - \hat{\mathbf{d}}_r. \tag{57}$$

Least mean squares adaptive filtering for estimating $d_{ur}(n)$ falls within the realm of linear filtering, though time-varying, with $r(n)$ serving as the reference signal [123], [124]. The order of the finite impulse response filter and the adaptation constant constitute the crucial design parameters. In a later study, it was demonstrated that initial smoothing of $d(n)$ and $r(n)$ is crucial to make this technique work [117].

A potential disadvantage with the linear filtering approach is that it operates independently of whether the cardiorespiratory coupling is significant or not. By conditioning filtering on the presence of cardiorespiratory coupling, this disadvantage may be addressed [120]. The coupling can be assessed using Granger's causality test, determining whether knowledge about past samples of $r(n)$ improves the prediction of $d(n)$, supported by a statistical significance test [120], [125]. Alternatively, assessment can build on the assumption that a bivariate AR model describes the interaction between $d(n)$ and $r(n)$ [62]; coupling is then assessed using cross entropy which involves the variance of $d(n)$ and the variance of the residuals of the regression between $d(n)$ and the history of $r(n)$ [126]. Other approaches to assessing cardiorespiratory coupling include phase synchronization [127], [128], [129] and causality-related decomposition using transfer entropy techniques [130], [131].

B. Orthogonal Subspace Projection

Orthogonal projection of $d(n)$ onto the subspace spanned by $r(n)$ can also be considered without explicitly referring to filtering and least squares estimation [121], see also [62]. Although the matrix defining the subspace in these two studies differs from $\mathbf{R}_1$ as the order of the columns is reverted,

$$\mathbf{R}_2 = \begin{bmatrix} r(0) & r(1) & \cdots & r(p) \\ r(1) & r(2) & \cdots & r(p+1) \\ \vdots & \vdots & \ddots & \vdots \\ r(N-p-1) & r(N-p) & \cdots & r(N-1) \end{bmatrix}, \tag{58}$$

the projection matrix $\mathbf{P}_2$ associated with $\mathbf{R}_2$ is identical to $\mathbf{P}_1$ since $\mathbf{R}_2 = \mathbf{R}_1\mathbf{J}$, where $\mathbf{J}$ is the reversal matrix. Thus, although not previously noted in the literature, the decomposition based on $\mathbf{R}_2$, described in [62], [121], is identical to the decomposition based on $\mathbf{R}_1$, described in [116], [117], [120]. Figure 12 illustrates the signal decomposition resulting in $\hat{d}_{ur}(n)$ which largely lacks the oscillations due to respiration.

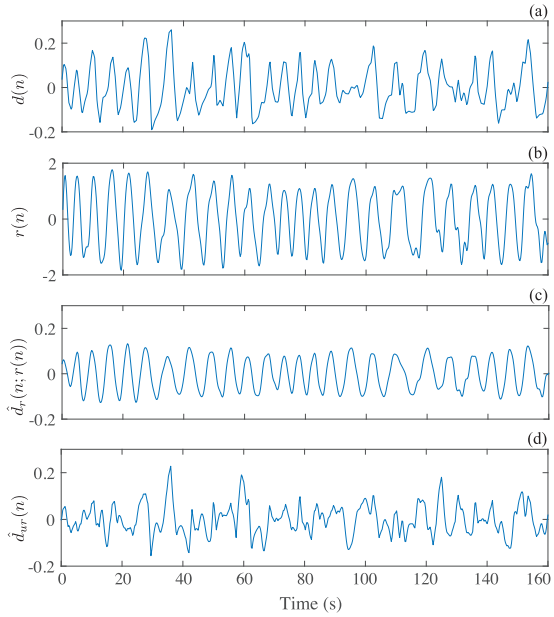

Fig. 12. Signal decomposition using orthogonal subspace projection. (a) $d(n)$ (here given by a sampled version of $\hat{m}(t)$ in (19)), (b) $r(n)$, (c) $\hat{d}_r(n;r(n))$ and (d) $\hat{d}_{ur}(n)$. The ECG was recorded during relaxing audio listening [105]. The vertical scales have arbitrary units.

Rather than constructing $\mathbf{R}_2$ directly from $r(n)$, a multiscale approach has been proposed in which $\mathbf{R}_2$ is constructed from the detail coefficients of wavelet analysis, using the Daubechies-4 wavelet at five different scales [117], see also [132]. The wavelet-based matrix is then given by

$$\mathbf{R}_3 = \begin{bmatrix} \mathbf{w}_{1,p} & \cdots & \mathbf{w}_{1,1} & \mathbf{w}_{2,p} & \cdots & \mathbf{w}_{2,1} & \cdots & \mathbf{w}_{5,1} \end{bmatrix}, \tag{59}$$

where

$$\mathbf{w}_{l,n} = \begin{bmatrix} w_l(n) & w_l(n+1) & \cdots & w_l(n+N-1) \end{bmatrix}^T,$$

and $w_l(n)$ is the l-th detail scale of $r(n)$.

C. Smoothed Extended Kalman Filtering

A more advanced approach to decomposing $d(n)$ is based on a model which resembles the time-varying autoregressive, moving average model with exogenous input, involving $d(n)$, $r(n)$, and $d_{ur}(n)$ [68]. The approach differs from those leading up to orthogonal subspace projection as it is statistical in nature. The HRV signal $d(n)$ is modeled by a sum of a respiration-related component $d_r(n;r(n))$, a respiration-unrelated component $d_{ur}(n)$, and observation noise $v(n)$,

$$d(n) = d_r(n;r(n)) + d_{ur}(n) + v(n), \tag{60}$$

where $d_r(n;r(n))$ is a filtered version of the exogenous input $r_s(n)$,

$$d_r(n;r(n)) = \sum_{k=0}^{p} b(k,n)r_s(n-k), \tag{61}$$

and $d_{ur}(n)$ is described by a time-varying AR model driven by white noise $e(n)$,

$$d_{ur}(n) = \sum_{k=1}^{q} a(k,n) d_{ur}(n-k) + e(n). \tag{62}$$

The dominant respiratory component $r_s(n)$ is modeled by a sinusoidal with amplitude $a_r^2(n)$, fundamental frequency $\theta_r(n; f_r(n))$, and phase $\varphi_r(n)$,

$$r_s(n) = a_r^2(n) \sin(\theta_r(n; f_r(n)) + \varphi_r(n)). \tag{63}$$

The observed respiration signal is modeled by

$$r(n) = r_s(n) + r_{ns}(n) + v_r(n), \tag{64}$$

where $r_{ns}(n)$ represents the non-sinusoidal components of $r(n)$ and $v_r(n)$ is white noise.

The model equations (60)–(64) can be assembled in the following state-space representation:

$$\mathbf{x}(n+1) = f(\mathbf{x}(n)) + \mathbf{w}(n),$$
$$\mathbf{y}(n) = g(\mathbf{x}(n)) + \mathbf{v}(n),$$

where $f(\cdot)$ and $g(\cdot)$ are nonlinear functions. The state vector $\mathbf{x}(n)$ contains the following elements: $b(0,n), \ldots, b(p,n)$, $a(1,n), \ldots, a(q,n), d_{ur}(n), a_r(n), \theta_r(n; f_r(n)), f_r(n), \varphi_r(n)$, and $r_{ns}(n)$. The observation vector $\mathbf{y}(n)$ contains $d(n)$ and $r(n)$. A simple random walk model accounts for the variation of each element in $\mathbf{x}(n)$. The vectors $\mathbf{w}(n)$ and $\mathbf{v}(n)$ represent the system and observation noise, respectively.

Once the state-space equations have been defined, the model orders p and q are estimated and the initial values of the state vector and noise variances determined, the smoothed extended Kalman filter can be used to estimate $\mathbf{x}(n)$ [68]. Clearly, to run the filter, numerous values need first to be determined, most of them based on experiential knowledge.

Using the smoothed extended Kalman filter, operating both forward and backward in time, the decomposed spectra of $\hat{d}_r(n; r(n))$ and $\hat{d}_{ur}(n)$ can be computed directly from $\hat{a}(k,n)$ and $\hat{b}(k,n)$, respectively, see Fig. 13. The two decomposed spectra essentially coincide with the original spectra in the LF and HF bands, except for some overlap around 0.2 Hz.

D. Empirical Mode Decomposition

Empirical mode decomposition was originally used to decompose $d(n)$ without any involvement of $r(n)$, see, e.g., [133]. However, respiration-guided decomposition has later been proposed in which $d(n)$ is decomposed into a sum of intrinsic mode functions $c_i(n)$ plus a residual $c_r(n)$ [134],

$$d(n) = \sum_{i=1}^{I} c_i(n) + c_r(n), \tag{65}$$

where I is the number of intrinsic mode functions. To determine whether $d(n)$ and $r(n)$ are coupled, each $c_i(n)$ is crosscorrelated to a respiratory-derived signal $r_s(n)$ reflecting the average slope of $r(n)$ in each heartbeat. The signal $r_s(n)$ is obtained by differencing $r(n)$ at the time of successive R-wave peaks, followed by equidistant resampling to the same rate as that of $d(n)$. Due to the differencing, $r_s(n)$ emphasizes short-term variation in respiration, while low-frequency drift unrelated to HRV is essentially filtered out.

The desired respiration-related signal $d_r(n)$ is obtained by summing those $c_i(n)$ whose crosscorrelation with $r_s(n)$ is statistically significant; conversely, $d_{ur}(n)$ is obtained by summing those $c_i(n)$ not associated with statistically significance.

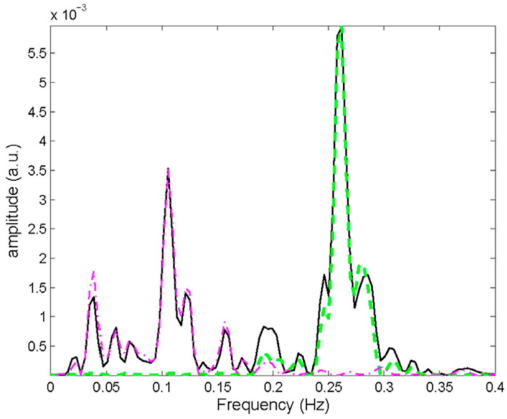

Fig. 13. Decomposition of the power spectrum of $d(n)$ (black line) into the spectra of $\hat{d}_{ur}(n)$ and $\hat{d}_r(n; r(n))$ (purple and green line, respectively), using the smoothed extended Kalman filter. The ECG was recorded from a healthy subject during normal respiration. Reprinted from [68] with permission.

E. Decomposition-Based HRV Indices

The decomposition of $\mathbf{d}$ into $\hat{\mathbf{d}}_r$ and $\hat{\mathbf{d}}_{ur}$ opens up for the definition of HRV indices which address limitations of existing spectral indices. The normalized power of $\hat{\mathbf{d}}_r$ and $\hat{\mathbf{d}}_{ur}$ are two simple but useful indices [121], defined by

$$P_r' = \frac{\hat{\mathbf{d}}_r^T \hat{\mathbf{d}}_r}{\hat{\mathbf{d}}^T \hat{\mathbf{d}}}, \quad P_{ur}' = \frac{\hat{\mathbf{d}}_{ur}^T \hat{\mathbf{d}}_{ur}}{\hat{\mathbf{d}}^T \hat{\mathbf{d}}}, \tag{66}$$

where P_r' mainly reflects respiratory sinus arrhythmia and parasympathetic activity, whereas P_{ur}' reflects respiration-unrelated fluctuations.

To partially address the criticism against the standard LF/HF ratio, here denoted $\mathcal{R}_s$, when used to assess sympathovagal balance [135], [136], a decomposition-based version of this index has been proposed [121], defined by

$$\mathcal{R} = \frac{P_{ur,\mathrm{LF}}}{P_{r,\mathrm{LF+HF}}}, \tag{67}$$

where $P_{ur,\mathrm{LF}}$ is the power of $d_{ur}(n)$ in the LF band and $P_{r,\mathrm{LF+HF}}$ is the power of $d_r(n)$ in the combined LF and HF bands. The performance of $\mathcal{R}$ has been evaluated in a study where one of the aims was to discriminate between a relax stage and five different stress stages, defined by the modified Trier Social Stress Test including memory tasks and emotional stress [121]. For a data set of 46 volunteers, Fig. 14 presents the distributions of $\mathcal{R}$ and $\mathcal{R}_s$ for the different stages. The results show that $\mathcal{R}$ differs with statistical significance between the relax stage and four of the

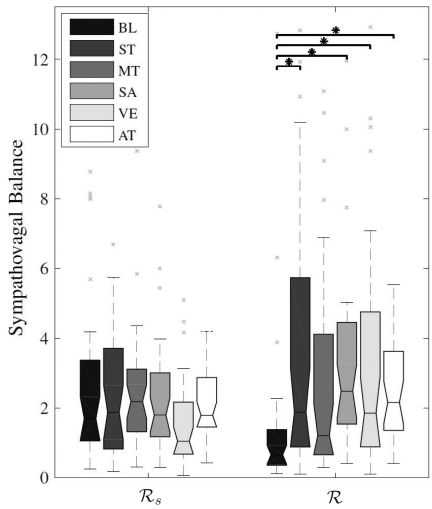

Fig. 14. Characterization of sympathovagal balance using the standard LF/HF ratio $\mathcal{R}_s$ and the decomposition-based $\mathcal{R}$, defined in (67), during a modified Trier Social Stress Test, including a baseline relax stage (BL), followed by stages of story telling (ST), memory task (MT), stress anticipation (SA), video exposition (VE), and arithmetic task (AT). The asterisk indicates $p < 0.003$. Reprinted from [121] with permission.

five stress stages, while $\mathcal{R}_s$ does not differ for any of the stress stages due to that respiration overlaps with the LF band in the relax stage [105].

The index $\mathcal{R}$ may assume unreasonably large values when the cardiorespiratory coupling is weak, a limitation which can be mitigated by normalizing $\mathcal{R}$ to become [134]

$$\mathcal{R}' = \frac{P_{ur,\mathrm{LF}}}{P_{r,\mathrm{LF+HF}} + P_{ur,\mathrm{LF}}}. \tag{68}$$

Thus, $\mathcal{R}'$ resembles the standard normalized ratio where the spectral power in the LF band is normalized with the spectral power of the bands combined.

VIII. Discussion

The present survey aims at highlighting the progress made with regard to methods which by design can handle time-varying conditions and the presence of confounding factors—aspects which undermine the interpretation of classical spectral analysis. Clearly, time–frequency analysis addresses the often unrealistic assumption of stationarity implied by classical spectral analysis. However, of central importance is also the emergence of time-varying, nonlinear signal processing techniques to represent heart rhythm with a time-varying mean heart rate, to correct ectopic beats, to redefine the frequency bands, to decompose the HRV signal by making use of a respiration signal, and more. Indeed, this development suggests that the spectral approach is not yet down for the count, but significant information can be extracted in the presence of rapid and transient changes or spectrally overlapping coactivation of the two ANS branches. Hence, the ongoing development of methods for time-varying processing is most likely bound to continue.

A major challenge in developing methods for HRV analysis is that the ground truth is rarely available, complicating evaluation and comparison of performance. For example, in ectopic beat correction, the accuracy of the estimated event time of the replaced beat cannot be established since the true event time by definition is unknown. In respiration-guided signal decomposition the accuracy of $\hat{d}_r(n; r(n))$ and $\hat{d}_{ur}(n)$ cannot be evaluated since the ground truth is unknown. Historically, this challenge has been addressed by evaluating performance indirectly, e.g., by judging to what extent the behavior of the LF and/or HF bands agree with the expected results. With regard to signal decomposition, performance has been evaluated indirectly in terms of statistical significance of indices which characterize different stages of a stress test.

A complementary approach to evaluating performance is to make use of simulated signals which exhibit characteristics of particular relevance to the problem addressed. As noted in Section II-A, the IPFM model has been used extensively for simulation purposes as well as for the development of model-based signal processing. The former aspect is exemplified by a recent study which compares the performance of different methods quantifying respiratory sinus arrhythmia [62]. In that study, the modulation function $m(t)$ was composed of two components: one taken as a real respiration signal and another produced by filtered white noise unrelated to respiration. To use simulated data is valuable as various statistical performance measures can be determined, however, simulated data is an idealization—something which is particularly true when the simulation model represents the point of departure for developing the method to be evaluated. Therefore, it is essential that results based on simulated data are paired with results based on real data to demonstrate the physiological or clinical significance.

The search for better heart rhythm representations has essentially come to an end as most recent efforts date back to some 10–15 years [77], [79]. Interestingly, both these studies proposed time-varying representations based on the IPFM model, one developed within a deterministic framework and another within a statistical, with both representations offering significant advantages over the classical representations. The heart timing representation provides an expression of the modulation function in terms of a time-varying mean heart rate, cf. (23), requiring only a modest amount of computations which is of the same order as the commonly used $d_{\mathrm{IIF}}(t)$, i.e., interpolation, resampling, and, possibly, linear, time-invariant filtering. The point process representation provides instantaneous estimates of both the mean RR interval and the mean heart rate (and related standard deviations) as well as an assessment of how well the model fits the observed data using a statistical test; to gain this information, a considerably larger amount of computations is required due to multi-parameter optimization and model order selection. It remains to be demonstrated which of the two frameworks is to be preferred, thus leaving room for future research which should investigate performance in engineering terms as well as in clinical terms.

While the analysis of rapid and transient HRV changes calls for proper tools [1], the classical representations, not accounting for mean heart rate, nonetheless continue to dominate in the literature. The model-based heart rhythm representations, much better suited to handle transient conditions, have yet to find their way into clinical HRV studies.

Of the processing steps described in this survey, ectopic beat correction is likely the least critical to embrace a time-varying

formulation, the main reason being that occasional ectopic beats are to be corrected, whereas longer segments with frequent ectopic beats are excluded from further analysis. This observation may explain why the model-based techniques described in Sections IV-A to IV-C have not been extended to handle time-varying conditions. On the other hand, such handling is inherent to the point process method. Using artificially corrupted RR interval series, the performance of the point process method was compared to that of the simplified correction based on the heart timing signal (Section IV-C): the median of the root mean square error between the estimated and the true event time of a missing beat was found to be quite similar (12.1 ms and 15.7 ms, respectively) [96].

The influence of respiration, being a major confounder in HRV analysis, can be dealt with in various ways by, e.g., redefining the HF band by means of the respiratory frequency (Section V-A), performing model-based estimation of the LF and HF components using respiratory frequency (Section VI), and performing spectral analysis of signals obtained by respiration-guided decomposition (Section VII). Redefinition of the HF band based on the respiratory frequency offers a viable solution in certain situations, while not so when the respiration-related spectral content overlaps with the LF band. Of the three just mentioned approaches, signal decomposition is probably the more controversial to perform, one reason being that "adjusting HRV measurements for confounders that are also under autonomic control might affect their predictive value" [137]. However, this statement should be counterbalanced by the results presented in some of the studies referred to in Section VII. For example, the results in Fig. 14 show that the desired decomposed signal actually contains information which, when used to form the index $\mathcal{R}$, can distinguish the relax stage from most of the stress stages.

It should be noted that while non-adjusted HRV indices may have predictive value, their interpretation can be completely misleading. For example, a high normalized LF power due to a very low respiratory rate can certainly discriminate between different groups of subjects but lead to the erroneous interpretation of sympathetic dominance.

Respiration-guided decomposition has a place in the HRV analysis toolbox, however, various aspects deserve further investigation, for example, the relation between respiratory signal quality and decomposition performance. In the context of assessing ANS response to pharmacological blockade and stress, recent results suggest that similar performance can be achieved irrespective of whether real or ECG-derived signals are used [37]. Regarding the quality of ECG-derived signals, it is important to select among those lead(s) which better reflect the respiration-modulated changes in the ECG.

Most methods proposed for respiration-guided decomposition rest on the assumption that the cardiorespiratory coupling is always present. Since this assumption is not always valid, it would be valuable to either establish how such methods perform when coupling is weak, and, if warranted, modify the method so that weak coupling is handled properly, for example, by considering the approaches proposed in [62], [120]. Using simulated data, a recent study investigated cardiorespiratory coupling with regard to, e.g., the filter order p and the phase delay between the HRV and respiratory signals [138].

Another aspect on respiration-guided decomposition relates to the handling of time-varying conditions. While the smoothed Kalman filter by design can handle such conditions, orthogonal subspace projection is derived from the assumption that respiration-related HRV signal $d_r(n; r(n))$ is related to the respiration signal $r(n)$ through time-invariant filtering, cf. (53), suggesting that the projection in (56) is also time-invariant. However, it is important to realize that estimation of $d_r(n; r(n))$ by orthogonal projection also results in time-varying filtering of $d(n)$ [24]. Even so, the projection matrix may require to be recomputed in successive windows to deal with that the coupling between respiration and HRV can vary over time. With the growing number of techniques developed for estimating $d_r(n; r(n))$ and the residual signal $d_{ur}(n)$, performance benchmarking is highly warranted. The techniques used for respiration-guided decomposition may be modified for the purpose of eliminating the HRV component due to pedaling or running, provided that external signal information is available on pedaling or running. Whether this idea is feasible remains to be investigated.

Algorithmic complexity plays a role when long-term ECG recordings are of interest to analyze, especially in light of that certain methods tend to be computationally demanding—an aspect which only recently has received some attention. For example, a 50 times difference in execution time between methods for estimating respiratory sinus arrhythmia has been reported, where orthogonal subspace projection was found to be one of the fastest methods [62]. Another algorithmic aspect is the number of design parameters that need to be set before operation: while orthogonal subspace projection involves just one parameter, i.e., the filter order, the smoothed Kalman filter involves a large number of parameters [68]. As the number of parameters grows, it becomes increasingly important to investigate to what extent performance is influenced when using slightly different parameter settings.

While the clinical implications of time-varying HRV analysis have yet to be demonstrated in clinical trials, the significance of such analysis is well-established by several experimental studies. Time-varying analysis is essential when characterizing the dynamics of the autonomic response, especially in the presence of time-varying mean heart and respiratory rates observed in experiments with Valsalva maneuver and cold pressure testing [139], normal and pathological sleep screening [140], induced emotions [141], exercise testing [79], pharmacological interventions [142], and driver drowsiness detection [143]. Indeed, it has been shown that not only are most signals recorded during a tilt table test nonstationary, but so are many recorded during resting supine and standing positions [10].

IX. Conclusion

Spectral analysis of HRV has advanced considerably from its inception to become a smorgasbord of methods which makes it possible to handle time-varying conditions as well as several confounding factors and spurious components. Nonetheless, before performing spectral analysis, the conditions under which

the HRV signal is acquired must be carefully scrutinized to ensure that adequate methods are employed. It is equally critical to account for a mean heart rate which varies markedly over time as it is restrict the analysis to frequencies below half the mean heart rate; if not, the comparison of HRV spectra may turn out meaningless. Despite the recent advancements, further research is needed on methods which make use of information on respiration as well as to benchmark the performance of different decomposition techniques.

References

[1] N. Montano et al., "Heart rate variability explored in the frequency domain: A tool to investigate the link between heart and behavior," *Neurosci. Biobehavioral Rev.*, vol. 33, pp. 71–80, 2009.

[2] D. S. Quintana and J. A. J. Heathers, "Considerations in the assessment of heart rate variability in biobehavioral research," *Front. Psychol.*, vol. 5, 2014, Art. no. 805.

[3] H. G. Kim et al., "Stress and heart rate variability: A meta-analysis and review of the literature," *Psychiatry Investigation*, vol. 15, pp. 235–245, 2018.

[4] B. M. A. Sayers, "Analysis of heart rate variability," *Ergonomics*, vol. 16, pp. 17–32, 1973.

[5] S. Akselrod et al., "Power spectrum analysis of heart rate fluctuations: A quantitative probe of beat-to-beat cardiovascular control," *Science*, vol. 213, pp. 220–222, 1981.

[6] B. Pomerantz et al., "Assessment of autonomic function in humans by heart rate espectral analysis," *Amer. J. Physiol.*, vol. 248, pp. H151–153, 1985.

[7] M. Pagani et al., "Power spectral analysis of heart rate and arterial pressure variabilities as a marker of sympatho-vagal interaction in man and concious dog," *Circulation Res.*, vol. 59, pp. 178–193, 1986.

[8] P. Laguna et al., "Power spectral density of unevenly sampled data by least-square analysis: Performance and application to heart rate signals," *IEEE Trans. Biomed. Eng.*, vol. 45, no. 6, pp. 698–715, Jun. 1998.

[9] J. Hayano and E. Yuda, "Pitfalls of assessment of autonomic function by heart rate variability," *J. Physiol. Anthropol.*, vol. 38, no. p. 1–8, 2019.

[10] M. Orini et al., "Assessment of the dynamic interactions between heart rate and arterial pressure by cross time–frequency analysis," *Physiol. Meas.*, vol. 33, pp. 315–331, 2012.

[11] D. A. Dickey and W. A. Fuller, "Distribution of the estimators for autoregressive time series with a unit root," *J. Amer. Stat. Assoc.*, vol. 74, pp. 427–431, 1979.

[12] P. Borgnat et al., "Testing stationarity with surrogates: A time–frequency approach," *IEEE Trans. Signal Process.*, vol. 58, no. 7, pp. 3459–3470, Jul. 2010.

[13] A. M. Bianchi et al., "Time-variant power spectrum analysis for the detection of transient episodes in HRV signal," *IEEE Trans. Biomed. Eng.*, vol. 40, no. 2, pp. 136–144, Feb. 1993.

[14] L. T. Mainardi, "On the quantification of heart rate variability spectral parameters using time–frequency and time-varying methods," *Philos. Trans. Roy. Soc. A*, vol. 367, pp. 255–275, 2009.

[15] M. Orini et al., "Time–frequency analysis of cardiovascular signals and their dynamic interactions," in *Complexity and Nonlinearity in Cardiovascular Signals*, R. Barbieri, E. P. Scilingo, and G. Valenza, Eds. New York City, NY, USA: Springer Int. Pub., 2017, ch. 9, pp. 257–287.

[16] A. Porta et al., "Entropy, entropy rate and pattern classification as tools to typify complexity in short heart period variability series," *IEEE Trans. Biomed. Eng.*, vol. 48, no. 11, pp. 1282–1291, Nov. 2001.

[17] A. Voss et al., "Methods derived from nonlinear dynamics for analysing heart rate variability," *Philos. Trans. Roy. Soc. A*, vol. 367, pp. 277–296, 2009.

[18] R. Sassi et al., "Advances in heart rate variability signal analysis: Joint position statement by the e-Cardiology ESC Working Group and the European Heart Rhythm Association co-endorsed by the Asia Pacific Heart Rhythm Society," *Europace*, vol. 17, pp. 1341–1353, 2015.

[19] G. E. Billman, "Heart rate variability–A historical perspective," *Front. Physiol.*, vol. 2, 2011, Art. no. 86.

[20] G. Ernst, "Hidden signals–The history and methods of heart rate variability," *Front. Public Health*, vol. 5, 2017, Art. no. 265.

[21] R. I. Kitney and O. Rompelman, Eds., *The Study of Heart Rate Variability*. Oxford, London: Clarendon Press, 1980.

[22] Task Force of The European Society of Cardiology and The North Americam Society for Pacing and Electrophysiology, "Heart rate variability: Standards of measurement, physiological interpretation, and clinical use," *Circulation*, vol. 93, pp. 1043–1065, 1996.

[23] M. Malik, "Standard measurements of heart rate variability," in *Dynamic Electrocardiography*, M. Malik and A. J. Camm, Eds. New York, NY,USA: Wiley–Blackwell, 2004, ch. 2, pp. 13–21.

[24] L. Sörnmo and P. Laguna, *Bioelectrical Signal Processing in Cardiac and Neurological Applications*. Amsterdam, The Netherlands: Elsevier Academic Press, 2005.

[25] U. R. Acharya et al., "Heart rate variability: A review," *Med. Biol. Eng. Comput.*, vol. 44, pp. 1031–1051, 2006.

[26] M. A. Peltola, "Role of editing of R–R intervals in the analysis of heart rate variability," *Front. Physiol.*, vol. 3, 2012, Art. no. 148.

[27] F. Shaffer et al., "A healthy heart is not a metronome: An integrative review of the heart's anatomy and heart rate variability," *Front. Psychol.*, vol. 5, 2014, Art. no. 1040.

[28] F. Shaffer and J. P. Ginsberg, "An overview of heart rate variability metrics and norms," *Front. Public Health*, vol. 5, 2017, Art. no. 258.

[29] N. Singh et al., "Heart rate variability: An old metric with new meaning in the era of using mhealth technologies for health and exercise training guidance. Part One: Physiology and methods," *Arrhythmia Electrophysiol. Rev.*, vol. 7, pp. 193–198, 2018.

[30] S. Massaro and L. Pecchia, "Heart rate variability (HRV) analysis: A methodology for organizational neuroscience," *Organizational Res. Methods*, vol. 22, pp. 354–393, 2019.

[31] G. B. Moody et al., "Derivation of respiratory signals from multi-lead ECG's," in *Proc. Comput. Cardiol.*, 1985, pp. 113–116.

[32] S. Leanderson et al., "Estimation of respiration frequency using spatial information from the VCG," *Med. Eng. Phys.*, vol. 25, pp. 501–507, 2003.

[33] R. Bailón et al., "A robust method for ECG-based estimation of the respiratory frequency during stress testing," *IEEE Trans. Biomed. Eng.*, vol. 53, no. 7, pp. 1273–1285, Jul. 2006.

[34] P. Langley et al., "Principal component analysis as a tool for analyzing beat-to-beat changes in ECG features: Application to ECG-derived respiration," *IEEE Trans. Biomed. Eng.*, vol. 57, no. 4, pp. 821–829, Apr. 2010.

[35] D. Widjaja et al., "Application of kernel principal component analysis for single-lead-ECG-derived respiration," *IEEE Trans. Biomed. Eng.*, vol. 59, no. 4, pp. 1169–1176, Apr. 2012.

[36] E. Helfenbein et al., "Development of three methods for extracting respiration from the surface ECG: A review," *J. Electrocardiol.*, vol. 47, pp. 819–825, 2014.

[37] C. Varon et al., "ECG-derived respiration for ambulatory monitoring using the single-lead ECG," *Sci. Rep.*, vol. 10, 2020, Art. no. 5704.

[38] A. Adami et al., "A new framework to estimate breathing rate from electrocardiogram, photoplethysmogram, and blood pressure signals," *IEEE Access*, vol. 9, pp. 45832–45844, 2021.

[39] R. Wilders, "Computer modelling of the sinoatrial node," *Med. Biol. Eng. Comput.*, vol. 45, pp. 189–207, 2007.

[40] A. Fabbri et al., "Computational analysis of the human sinus node action potential: Model development and effects of mutations," *J. Physiol.*, vol. 595, no. 7, pp. 2365–2396, 2017.

[41] P. Flandrin, *Explorations in Time-Frequency Analysis*. Cambridge, U.K.: Cambridge Univ. Press, 2018.

[42] B. W. Hyndman and R. K. Mohn, "A model of the cardiac pacemaker and its use in decoding the information content of cardiac intervals," *Automedica*, vol. 1, pp. 239–252, 1975.

[43] O. Rompelman et al., "The measurement of heart rate variability spectra with the help of a personal computer," *IEEE Trans. Biomed. Eng.*, vol. BME-29, no. 7, pp. 503–510, Jul. 1982.

[44] R. W. de Boer et al., "Spectrum of a series of point event, generated by the integral pulse frequency modulation model," *Med. Biol. Eng. Comput*, vol. 23, pp. 138–142, 1985.

[45] R. D. Berger et al., "An efficient algorithm for spectral analysis of heart rate variability," *IEEE Trans. Biomed. Eng.*, vol. BME-33, no. 9, pp. 900–904, Sep. 1986.

[46] B. J. TenVoorde et al., "Spectra of data sampled at frequency modulated rates in application to cardiovascular signals: Part 1 analytical derivation of the spectra," *Med. Biol. Eng. Comput*, vol. 32, pp. 63–70, 1994.

[47] P. Castiglioni, "Evaluation of heart rhythm variability by heart or heart period: Differences, pitfalls and help from logarithms," *Med. Biol. Eng. Comput.*, vol. 33, pp. 323–330, 1995.

[48] M. Nakao et al., "Spectral distortion properties of the integral pulse frequency modulation model," *IEEE Trans. Biomed. Eng.*, vol. 44, no. 5, pp. 419–426, May 1997.

[49] I. P. Mitov and I. K. Daskalov, "Comparison of heart rate variability spectra using generic relationships of their input signals," *Med. Biol. Eng. Comput.*, vol. 36, pp. 573–580, 1998.

[50] J. Mateo and P. Laguna, "Improved heart rate variability signal analysis from the beat occurrence times according to the IPFM model," *IEEE Trans. Biomed. Eng.*, vol. 47, no. 8, pp. 997–1009, Aug. 2000.

[51] G. B. Stanley et al., "Threshold modeling of autonomic control of heart rate variability," *IEEE Trans. Biomed. Eng.*, vol. 47, no. 9, pp. 1147–1153, Sep. 2000.

[52] I. P. Mitov, "Spectral analysis of heart rate variability using the integral pulse frequency modulation model," *Med. Biol. Eng. Comput*, vol. 39, pp. 348–354, 2001.

[53] H. Chiu and T. Kao, "A mathematical model for autonomic control of heart rate variation," *IEEE Eng. Med. Biol. Mag.*, vol. 20, no. 2, pp. 69–76, Mar./Apr. 2001.

[54] J. C. Echeverria et al., "Application of empirical mode decomposition to heart rate variability analysis," *Med. Biol. Eng. Comput.*, vol. 39, pp. 471–479, 2001.

[55] M. Brennan et al., "Poincaré plot interpretation using a physiological model of HRV based on a network of oscillators," *Amer. J. Physiol. Heart Circulatory Physiol.*, vol. 283, pp. H1873–H1886, 2002.

[56] H.-W. Chiu et al., "The influence of mean heart rate on measures of heart rate variability as markers of autonomic function: A model study," *Med. Eng. Phys.*, vol. 25, pp. 475–481, 2003.

[57] E. Pyetan and S. Akselrod, "Do the high-frequency indexes of HRV provide a faithful assessment of cardiac vagal tone? A critical theoretical evaluation," *IEEE Trans. Biomed. Eng.*, vol. 50, no. 6, pp. 777–783, Jun. 2003.

[58] D. Smith et al., "Model-based detection of heart rate turbulence using mean shape information," *IEEE Trans. Biomed. Eng.*, vol. 57, no. 2, pp. 334–342, Feb. 2010.

[59] H. Li et al., "Hilbert–Huang transform for analysis of heart rate variability in cardiac health," *IEEE/ACM Trans. Comput. Biol. Bioinf.*, vol. 8, no. 6, pp. 1557–1567, Nov./Dec. 2011.

[60] S. Chen and S. Chao, "Compressed sensing technology-based spectral estimation of heart rate variability using the integral pulse frequency modulation model," *IEEE J. Biomed. Health Inform.*, vol. 18, no. 3, pp. 1081–1090, May 2014.

[61] J. Bolea et al., "Influence of heart rate in non-linear HRV indices as a sampling rate effect evaluated on supine and standing," *Front. Physiol.*, vol. 7, 2016, Art. no. 501.

[62] J. F. Morales et al., "Model-based evaluation of methods for respiratory sinus arrhythmia estimation," *IEEE Trans. Biomed. Eng.*, vol. 68, no. 6, pp. 1882–1893, Jun. 2021.

[63] D. Candia-Rivera et al., "Integral pulse frequency modulation model driven by sympathovagal dynamics: Synthetic vs. real heart rate variability," *Biomed. Signal Process. Control*, vol. 68, 2021, Art. no. 102736.

[64] N. Satoh, "Spectral decomposition of heart rate variability using generalized harmonic analysis," *Biomed. Signal Process. Control*, vol. 70, 2021, Art. no. 103050.

[65] J. L. Folks and R. S. Chhikara, "The inverse Gaussian distribution and its statistical application–A review," *J. Roy. Stat. Soc. B*, vol. 40, pp. 263–289, 1978.

[66] J. G. Ruiz, "Introducing threshold modulation in Bayly's integral pulse frequency modulation in the neuron," *Proc. IEEE*, vol. 63, no. 4, pp. 733–735, Apr. 1975.

[67] S. R. Seydnejad and R. I. Kitney, "Time-varying threshold integral pulse frequency modulation," *IEEE Trans. Biomed. Eng.*, vol. 48, no. 9, pp. 949–962, Sep. 2001.

[68] L. S. Goldoozian et al., "Time-varying assessment of heart rate variability parameters using respiratory information," *Comput. Biol. Med.*, vol. 89, pp. 355–367, 2017.

[69] G. Baselli et al., "Autoregressive modeling and power spectral estimate of R-R interval time series in arrhythmic patients," *Comput. Biomed. Res.*, vol. 18, pp. 510–530, 1985.

[70] P. E. McSharry et al., "A dynamical model for generating synthetic electrocardiogram signals," *IEEE Trans. Biomed. Eng.*, vol. 50, no. 3, pp. 289–294, Mar. 2003.

[71] O. Meste et al., "Time-varying analysis methods and models for the respiratory and cardiac system coupling in graded exercise," *IEEE Trans. Biomed. Eng.*, vol. 52, no. 11, pp. 1921–1930, Nov. 2005.

[72] M. P. Tarvainen et al., "Time-varying analysis of heart rate variability signals with a Kalman smoother algorithm," *Physiol. Meas.*, vol. 27, pp. 225–239, 2006.

[73] R.-C. Peng et al., "Time–frequency analysis of heart rate variability during the cold pressor test using a time-varying autoregressive model," *Physiol. Meas.*, vol. 36, pp. 441–452, 2015.

[74] G. Dorantes-Méndez et al., "Time-varying analysis of the heart rate variability during A-phases of sleep: Healthy and pathologic conditions," *Biomed. Signal Process. Control*, vol. 40, pp. 111–116, 2018.

[75] A. L. Callara et al., "Parasympathetic–sympathetic causal interactions assessed by time-varying multivariate autoregressive modeling of electrodermal activity and heart-rate-variability," *IEEE Trans. Biomed. Eng.*, vol. 68, no. 10, pp. 3019–3028, Oct. 2021.

[76] M. Orini et al., "Synthesis of HRV signals characterized by predetermined time–frequency structure by means of time-varying ARMA models," *Biomed. Signal Process. Control*, vol. 7, pp. 141–150, 2012.

[77] R. Barbieri et al., "A point-process model of human heartbeat intervals: New definitions of heart rate and heart rate variability," *Amer. J. Physiol. Heart Circulatory Physiol.*, vol. 288, pp. H424–H435, 2005.

[78] Z. Chen et al., "Assessment of autonomic control and respiratory sinus arrhythmia using point process models of human heart beat dynamics," *IEEE Trans. Electromagn. Compat.*, vol. 56, no. 7, pp. 1791–1802, Jul. 2009.

[79] R. Bailón et al., "The integral pulse frequency modulation model with time-varying threshold: Application to heart rate variability analysis during exercise stress testing," *IEEE Trans. Biomed. Eng.*, vol. 58, no. 3, pp. 642–652, Mar. 2011.

[80] F. Hlawatsch and G. F. Boudreaux-Bartels, "Linear and quadratic time–frequency signal representations," *IEEE Signal Process. Mag.*, vol. 9, pp. 21–67, 1992.

[81] D. J. Daley and D. Vere-Jones, *An Introduction to the Theory of Point Processes: Volume I: Elementary Theory and Methods*, 2nd ed. New York, NY, USA: Springer, 2003.

[82] E. N. Brown et al., "The time-rescaling theorem and its application to neural spike train data analysis," *Neural Comput.*, vol. 14, pp. 325–346, 2002.

[83] R. Barbieri and E. N. Brown, "Analysis of heartbeat dynamics by point process adaptive filtering," *IEEE Trans. Biomed. Eng.*, vol. 53, no. 1, pp. 4–12, Jan. 2006.

[84] M. N. Cheung, "Detection of recovery from errors in the cardiac interbeat intervals," *Psychophysiology*, vol. 18, pp. 341–346, 1981.

[85] P. Albrecht and R. J. Cohen, "Estimation of heart rate power spectrum bands from real world data: Dealing with ectopic beats and noise data," in *Proc. Comput. Cardiol.*, 1988, pp. 311–314.

[86] L. J. M. Mulder, "Measurement and analysis methods of heart rate and respiration for use in applied environments," *Biol. Psychol.*, vol. 34, pp. 205–236, 1992.

[87] N. Lippman et al., "Comparison of methods for removal of ectopy in measurements of heart rate variability," *Amer. J. Physiol.*, vol. 267, pp. H411–H418, 1994.

[88] R. A. Thuraisingham, "Preprocessing RR interval time series for heart rate variability analysis and estimates of standard deviation of RR intervals," *Comput. methods Programs Biomed.*, vol. 83, pp. 78–82, 2006.

[89] J. Rand et al., "Realtime correction of heart interbeat intervals," *IEEE Trans. Biomed. Eng.*, vol. 54, no. 5, pp. 946–950, May 2007.

[90] M. Karlsson et al., "Automatic filtering of outliers in RR intervals before analysis of heart rate variability in holter recordings: A comparison with carefully edited data," *Biomed. Eng. Online*, vol. 11, no. 1, pp. 1–12, 2012.

[91] A. Choi and H. Shin, "Quantitative analysis of the effect of an ectopic beat on the heart rate variability in the resting condition," *Front. Physiol.*, vol. 9, 2018, Art. no. 922.

[92] M. Brennan et al., "A new model-based ectopic beat correction algorithm for heart rate variability," in *Proc. Conf. Proc. 23rd Annu. Int. Conf. IEEE Eng. Med. Biol. Soc.*, 2001, vol. 1, pp. 567–570.

[93] O. Rompelman et al., "Measurement of heart-rate variability: Part 1—Comparative study of heart-rate variability analysis methods," *Med. Biol. Eng. Comput.*, vol. 15, pp. 239–252, 1977.

[94] J. Mateo and P. Laguna, "Analysis of heart rate variability in the presence of ectopic beats using the heart timing signal," *IEEE Trans. Biomed. Eng.*, vol. 50, no. 3, pp. 334–343, Mar. 2003.

[95] K. Solem et al., "An efficient method for handling ectopic beats using the heart timing signal," *IEEE Trans. Biomed. Eng.*, vol. 53, no. 1, pp. 13–20, Jan. 2006.

[96] L. Citi et al., "A real-time automated point process method for detection and correction of erroneous and ectopic heartbeats," *IEEE Trans. Biomed. Eng.*, vol. 59, no. 10, pp. 2828–2837, Oct. 2012.

[97] L. Keselbrener and S. Akselrod, "Selective discrete Fourier transform algorithm for time–frequency analysis: Method and application on simulated and cardiovascular signals," *IEEE Trans. Biomed. Eng.*, vol. 43, no. 8, pp. 789–802, Aug. 1996.
[98] S. Jasson et al., "Instant power spectrum analysis of heart rate variability during orthostatic tilt using a time-/frequency-domain method," *Circulation*, vol. 96, pp. 3521–3526, 1997.
[99] B. Pilgram and M. D. Renzo, "Estimating respiratory rate from instantaneous frequencies of long term heart rate tracings," in *Proc. Comput. Cardiol.*, 1993, pp. 859–862.
[100] E. Toledo et al., "Wavelet analysis of instantaneous heart rate: A study of autonomic control during thrombolysis," *Amer. J. Physiol. Regulatory Integrative Comp. Physiol.*, vol. 284, pp. R1079–R1091, 2003.
[101] R. Bailón et al., "Analysis of heart rate variability using time-varying frequency bands based on respiratory frequency," in *Proc. IEEE Conf. Eng. Med. Biol.*, 2007, vol. 29, pp. 6674–6677.
[102] R. Bailón et al., "Analysis of heart rate variability during exercise stress testing using respiratory information," *Biomed. Signal Process. Control*, vol. 5, pp. 299–310, 2010.
[103] Y. Goren et al., "Individual time-dependent spectral boundaries for improved accuracy in time–frequency analysis of heart rate variability," *IEEE Trans. Biomed. Eng.*, vol. 53, no. 1, pp. 35–42, Jan. 2006.
[104] M. T. Valderas Yamuza et al., "Human emotion characterization by heart rate variability analysis guided by respiration," *IEEE J. Biomed. Health Inform.*, vol. 23, no. 6, pp. 2446–2454, Nov. 2019.
[105] A. Hernando et al., "Inclusion of respiratory frequency information in heart rate variability analysis for stress assessment," *IEEE J. Biomed. Health Inform.*, vol. 20, no. 4, pp. 1016–1025, Jul. 2016.
[106] L. B. White and B. Boashash, "Cross spectral analysis of nonstationary processes," *IEEE Trans. Inform. Theory*, vol. 36, no. 4, pp. 830–835, Jul. 1990.
[107] M. Orini et al., "Characterization of dynamic interactions between cardiovascular signals by time–frequency coherence," *IEEE Trans. Biomed. Eng.*, vol. 59, no. 3, pp. 663–673, Mar. 2012.
[108] L. Faes et al., "Surrogate data analysis for assessing the significance of the coherence function," *IEEE Trans. Biomed. Eng.*, vol. 51, no. 7, pp. 1156–1166, Jul. 2004.
[109] G. Blain et al., "Time–frequency analysis of heart rate variability reveals cardiolocomotor coupling during dynamic cycling exercise in humans," *Amer. J. Physiol. Heart Circulatory Physiol.*, vol. 296, pp. H1651–H1659, 2009.
[110] K. Niizeki and T. Saitoh, "Cardiolocomotor phase synchronization during rhythmic exercise," *J. Phys. Fitness Sports Med.*, vol. 3, pp. 11–20, 2014.
[111] D. Hernando et al., "Methodological framework for heart rate variability analysis during exercise: Application to running and cycling stress testing," *Med. Biol. Eng. Comput.*, vol. 56, pp. 781–794, 2018.
[112] R. Bailón et al., "Influence of running stride frequency in heart rate variability analysis during treadmill exercise testing," *IEEE Trans. Biomed. Eng.*, vol. 60, no. 7, pp. 1796–1805, Jul. 2013.
[113] L. T. Mainardi et al., "Automatic decomposition of Wigner distribution and its application to heart rate variability," *Meth. Inf. Med.*, vol. 43, pp. 17–21, 2004.
[114] O. Anosov et al., "High-frequency oscillations of the heart rate during ramp load reflect the human anaerobic threshold," *Eur. J. Appl. Physiol.*, vol. 83, pp. 388–394, 2000.
[115] G. Blain et al., "Influences of breathing patterns on respiratory sinus arrhythmia in humans during exercise," *Amer. J. Physiol. Heart Circulatory Physiol.*, vol. 288, pp. H887–H895, 2005.
[116] J. Choi and R. Gutierrez-Osuna, "Removal of respiratory influences from heart rate variability in stress monitoring," *IEEE Sensors J.*, vol. 11, no. 11, pp. 2649–2565, Nov. 2011.
[117] D. Widjaja et al., "Separation of respiratory influences from the tachogram: A methodological evaluation," *PLoS One*, vol. 9, 2014, Art. no. e101713.
[118] L. Bernardi et al., "Effect of rosary prayer and yoga mantras on autonomic cardiovascular rhythms: Comparative study," *BMJ*, vol. 323, pp. 1446–1449, 2001.
[119] T. Penzel et al., "Modulations of heart rate, ECG, and cardio-respiratory coupling observed in polysomnography," *Front. Physiol.*, vol. 7, 2016, Art. no. 460.
[120] G. Lenis et al., "Separating the effect of respiration on the heart rate variability using Granger's causality and linear filtering," *Biomed. Signal Process. Control*, vol. 31, pp. 272–287, 2017.
[121] C. Varon et al., "Unconstrained estimation of HRV indices after removing respiratory influences from heart rate," *IEEE J. Biomed. Health Inform.*, vol. 23, no. 6, pp. 2386–2397, Nov. 2019.
[122] T. K. Moon and W. C. Sterling, *Mathematical Methods and Algorithms for Signal Processing*. Hoboken, NJ, USA: Prentice Hall, 2000.
[123] M. Varanini et al., "Adaptive filtering for cancelling/enhancing the respiratory contribution to cardiovascular signals," *J. Ambulatory Monit.*, vol. 5, pp. 95–105, 1992.
[124] S. Tiinanen et al., "Reducing the effect of respiration in baroreflex sensitivity estimation with adaptive filtering," *IEEE Trans. Biomed. Eng.*, vol. 55, no. 1, pp. 51–59, Jan. 2008.
[125] C. W. J. Granger, "Investigating causal relations by econometric models and cross-spectral methods," *Econometrica*, vol. 37, pp. 424–443, 1969.
[126] L. Faes et al., "Information decomposition in bivariate systems: Theory and application to cardiorespiratory dynamics," *Entropy*, vol. 17, pp. 277–303, 2015.
[127] E. Toledo et al., "Does synchronization reflect a true interaction in the cardiorespiratory system?," *Med. Eng. Phys.*, vol. 24, pp. 45–52, 2002.
[128] R. Bartsch et al., "Experimental evidence for phase synchronization transitions in the human cardiorespiratory system," *Phys. Rev. Lett.*, vol. 98, 2007, Art. no. 054102.
[129] B. Cairo et al., "Optimizing phase variability threshold for automated synchrogram analysis of cardiorespiratory interactions in amateur cyclists," *Philos. Trans. A. Math. Phys. Eng. Sci.*, vol. 379, 2021, Art. no. 20200251.
[130] D. Widjaja et al., "Cardiorespiratory information dynamics during mental arithmetic and sustained attention," *PLoS One*, vol. 10, no. 10, 2015, Art. no. e0129112.
[131] A. Porta et al., "Paced breathing increases the redundancy of cardiorespiratory control in healthy individuals and chronic heart failure patients," *Entropy*, vol. 20, 2018, Art. no. 949.
[132] C. Varon et al., "A novel algorithm for the automatic detection of sleep apnea from single-lead ECG," *IEEE Trans. Biomed. Eng.*, vol. 62, no. 9, pp. 2269–2278, Sep. 2015.
[133] R. Balocchi et al., "Deriving the respiratory sinus arrhythmia from the heartbeat time series using empirical mode decomposition," *Chaos, Solitons Fractals*, vol. 20, pp. 171–177, 2004.
[134] B. Liu et al., "An improved method to evaluate heart rate variability based on time-variant cardiorespiratory relation," *J. Appl. Physiol.*, vol. 127, pp. 320–327, 2019.
[135] D. L. Eckberg, "Sympathovagal balance: A critical appraisal," *Circulation*, vol. 96, pp. 3224–3232, 1997.
[136] G. E. Billman, "The LF/HF ratio does not accurately measure cardiac sympathovagal balance," *Front. Physiol.*, vol. 4, 2013, Art. no. 26.
[137] M. Malik et al., "Assessing cardiac autonomic function via heart rate variability analysis requires monitoring respiration: Reply confounders of heart rate variability," *Europace*, vol. 18, pp. 1280–1281, 2016.
[138] J. Morales et al., "Technical aspects of cardiorespiratory estimation using subspace projections and cross entropy," *Physiol. Meas.*, vol. 42, 2021, Art. no. 115008.
[139] J. L. Ducla-Soares et al., "Wavelet analysis of autonomic outflow of normal subjects on head-up tilt, cold pressor test, valsalva manoeuvre and deep breathing," *Exp. Physiol.*, vol. 92, pp. 677–686, 2007.
[140] M. O. Mendez et al., "Sleep apnea screening by autoregressive models from a single ECG lead," *IEEE Trans. Biomed. Eng.*, vol. 56, pp. 2838–2850, Dec. 2009.
[141] M. Orini et al., "A method for continuously assessing the autonomic response to music-induced emotions through HRV analysis," *Med. Biol. Eng. Comput.*, vol. 48, pp. 423–433, 2010.
[142] Z. Chen et al., "Dynamic assessment of baroreflex control of heart rate during induction of propofol anesthesia using a point process method," *Ann. Biomed. Eng.*, vol. 39, pp. 260–276, 2011.
[143] J. Vicente et al., "Drowsiness detection using heart rate variability," *Med. Biol. Eng. Comput.*, vol. 54, pp. 927–937, 2016.